University „Dunărea de Jos” from Galați

Doctoral School of Fundamental Sciences and Engineering

ABSTRACT OF THE DOCTORAL THESIS WITH THE TITLE:

STUDY AND MODELING OF COLD PLASMA ELECTRICAL DISCHARGES AT ATMOSPHERIC PRESSURE. POWER SUPPLIES FOR THEIR PRODUCTION

p.h.d. student,

eng. Cristian – Victor Lungu

p.h.d. supervizor,

Prof. dr. ing. habil. Bogdan HNATIUC

Series I3 No6

GALAȚI, 2022

Universitatea „Dunărea de Jos” din Galați

Școala doctorală de Științe Fundamentale și Inginerești

ABSTRACT OF THE DOCTORAL THESIS WITH THE TITLE:

STUDY AND MODELING OF COLD PLASMA ELECTRICAL DISCHARGES AT ATMOSPHERIC PRESSURE. POWER SUPPLIES FOR THEIR PRODUCTION

p.h.d. student eng. Cristian – Victor LUNGU

Comision president: Prof. dr. eng. habil. Marian BARBU
“Dunărea de jos” University from Galați

p.h.d. supervizor, Prof. dr. eng. habil. Bogdan HNATIUC
Maritime University of Constanța

Scientific references: Prof. dr. eng. Radu BURLICĂ
"Gheorghe Asachi" Technical University of Iași

Conf. dr. eng. Sorin – Robertino SINTEA
Maritime University of Constanța

Conf. dr. eng. Ciprian VLAD
“Dunărea de jos” University from Galați

Series I3 No 6

GALAȚI

2022

CHAPTER 1. Cold plasma discharges, ignition, evolution and maintenance

Matter is found in nature in the form of four states of aggregation. The best known are three of them, namely the liquid, solid and gaseous states. The fourth state of aggregation of matter is plasma. At very high temperatures, molecules absorb a large amount of energy, causing them to move in a disordered manner. With the energy absorbed, they can decompose into atoms, and due to the disordered displacement, these atoms can decompose into ions and electrons. Thus, excessive heating of the material is always accompanied by ionization, the environment remaining electrically neutral. This ionized state is called plasma, [1], [2], [3], [4], [5], [6].

Plasma is a mixture of gases made up of neutral particles and electrically charged particles. Their weight is large enough to lead electromagnetic interactions to a collective behavior of the particle assembly, [1], [2], [3], [4], [5], [6].

The energy required for the transition from the gaseous state to the plasma state is produced by an electric field accelerating free electrons. This is the main determinant of the gas-plasma transition and is dominated by collisions, [1], [2], [3], [4], [5]. A very good example is the fluorescent tube, because one of the most common applications of plasma is its use as a source of light radiation. The electric discharge in gas, at relatively low pressures, forms a column of luminous plasma, occupying a large part of the length of the tube, [1], [2], [3], [4], [5], [6].

1.1. Cold plasma electric discharges

Due to the free electric charges, the plasma conducts the electric current and is strongly influenced by the presence of external magnetic fields. As a result of collisions between electrons and atoms, phenomena of excitation of atoms can occur, followed by the emission of electromagnetic radiation. When the energy of the electrons is high enough, the atoms are ionized, and new charges, both positive and negative, can be obtained, [7], [10], [11], [12].

In Figure 1.1. the characteristic voltage - current, U (I), is reprezented, zones 1, 2, 3, 4 from Figure 1.1 correspond to non-thermal plasma discharges and zone 5 corresponds to thermal plasma also called electric arc. Possible types of electrical discharges called "cold plasma" can be identified, these include Corona discharges, luminescent discharges, sliding electric discharges (GlidArc),[6], [14], [15].

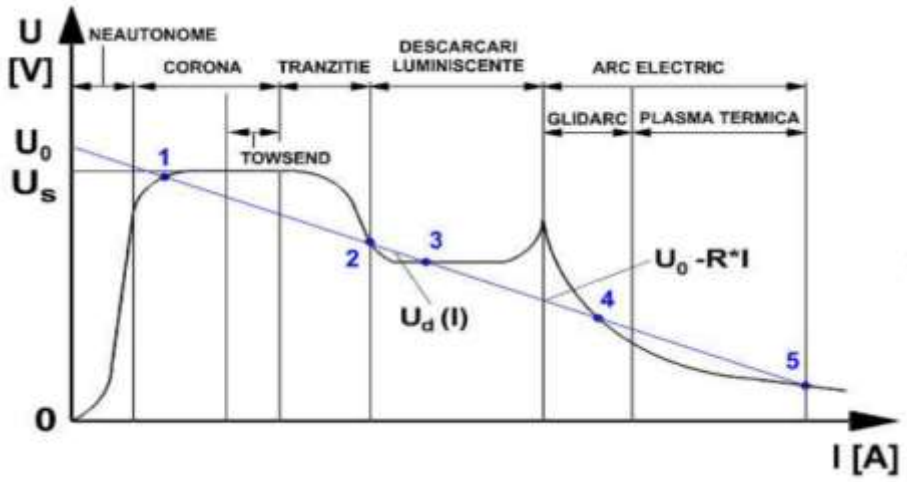

Figure 1.1. Electric discharges in steady state in relation to the volt-ampere characteristic,[7], [15]

In Table 1.1. the main parameters and conditions for initiating electric discharges for different types of discharges are presented, [7], [15].

Tabelul 1.1. Types of discharges, [7]

Type of discharge	U , [kV]	I , [A]	P , [atm]	T , [k]	χ	J, [A/cm^2]
Corona	>10	<10^{-5}	1	500	<10^{-6}	10^{-9}
DBD	100	<10^{-3}	1	500	<10^{-5}	10^{-5}
Luminescent	5	0,1	1	<500	<10^{-4}	10^{-3}
GlidArc	5-20	1	1	2000	<10^{-2}	1-10^2
Elecctric arc	0,03–0,05	10-10^3	1	>10000	10^{-2}-1	10^2-10^4

U - voltage
I - current
P - presure
T- temperature
χ - recombination factor
J - current density

1.2. Maintaining and autonomy of discharges

1.2.1. DC electric arc

The autonomous manifestation of discharges means their maintenance, even if the initial ionization phenomena, which underlie their initiation, cease. , [11], [13].

The volt-ampere characteristics of the electric arc can be static or dynamic, as the speed of variation of the current intensity through the arc is very small (particularly zero) or, on the contrary, has high values, [11], [13].

In Figure 1.2. the static volt-ampere characteristics of a dc electric arc are represented. , obtained for different constant column lengths. Table 1.2 shows the values of the coefficients in H. Ayrton's equation, [11], [13].

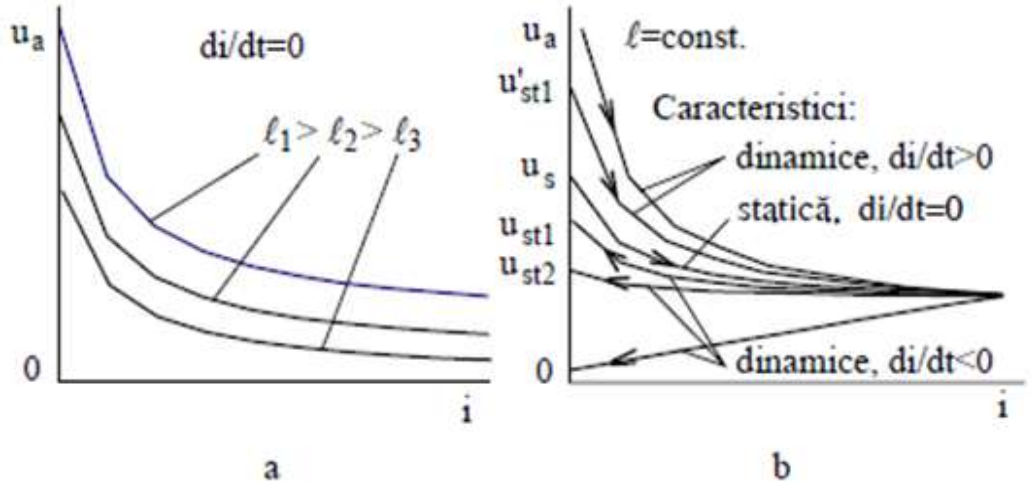

Figure 1.2. DC arc characteristics, [11]

a - static b – dynamic

In this sense, the approximation function given by Ayrton is known, having the expression, [11], [16]:

$$u_a(i) = a + \frac{b}{i} \tag{1.8}$$

where:

$$a=\alpha+\gamma\, l,\ b=\beta+\delta\, l \tag{1.10}$$

α,β,γ,δ, being constant, and *l* – the length of the electric arc column.

The approximation function proposed by Nottingham is also used in calculations, [11]:

$$u_a(i) = a + cl + (b + dl)i^{-n} \tag{1.11}$$

where *a*, *b*, *c*, *d* are constant, and *l* represents the length of the electric arc column.
The exponent n is calculated with the relation, [11] :

$$n = 2{,}62 \cdot 10^{-4}T \tag{1.12}$$

where T is the vaporization temperature of the anode, in absolute degrees.

Table 1.2. Values of the coefficients in the Ayrton function, [11]

	Coefficient			
Material	α, [V]	β, [VA]	γ, [V/m]	δ, [VA/m]
Copper	30	10	1000	3000
Carbon	39	11,7	21	105

Independența căderilor de tensiune la electrozi în raport cu lungimea *l* a coloanei arcului este considerată în funcția Rieder, care are expresia, [11]:

$$u_a(i) = \alpha + (\beta + l)\gamma\left[\ln\left(\frac{i}{\delta}\right)\right]^{-3} \tag{1.13}$$

α,β,γ,δ, fiind constante.

În Tabelul 1.3 sunt indicate valorile constantelor din funcția Rieder, [11].

Table 1.3. Values of the coefficients in the Rieder function, [11]

	Coefficient			
Material	α, [V]	β, [m]	γ, [V/m]	δ, [A]
Copper	26	0,013	$5{,}4 \cdot 10^5$	0,0074
Silver		0,011		
Wolfram		0,016		

1.2.2. AC electric arc

Unlike direct current electric arc, alternating current electric arc is a quasi-stationary process which, at unit length of the column, is characterized by a power balance equation. The modeling of the spring column can be done as in Figure 1.3, [11], [16].

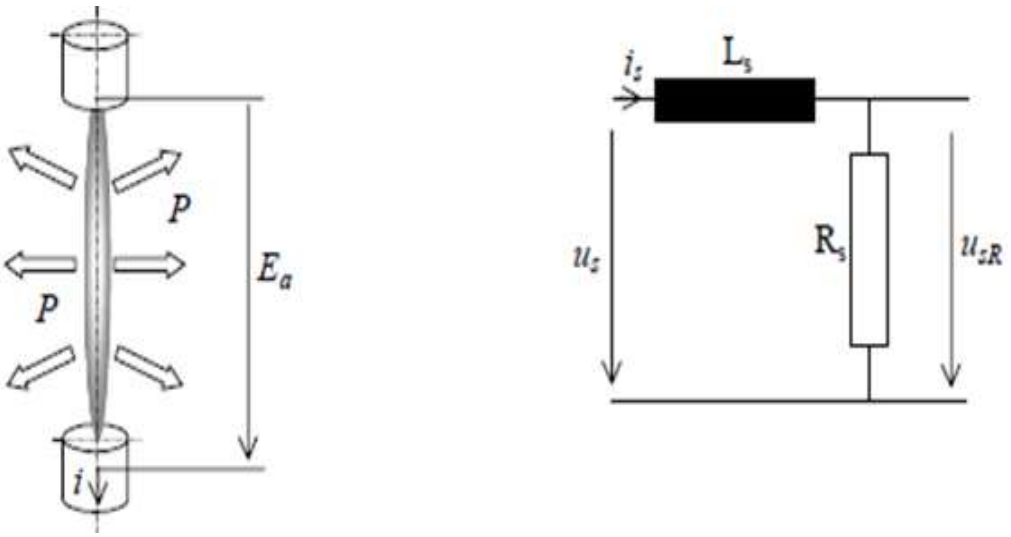

(a) *(b)*

Figure 1.3. Arc column modeling, alternating current, [11]

(a) Unitary length of the electric discharge column,
(b) Equivalent wiring diagram of the Mayr conductance model.
E_a – arc voltage; i- arc current;
P- the heat given to the environment in the unit of time.

The long electric arc is characterized by the fact that the phenomena in the arc column are dominant in relation to the phenomena that take place in the vicinity of the contact parts, so it is usually accepted for the arc voltage, Ua, a relation of form, [11], [16]:

$$U_a \cong E \cdot l \tag{1.14}$$

For long arc alternating current the phenomena that take place in the arc column before and after the natural zero crossing of the current can be described by Mayr's relation, which can be deduced by accepting the conductance of the electric arc, G_a (t), as, [11], [16]:

$$G_a(t) = \frac{i_a(t)}{u_a(t)} = k \cdot e^{\frac{Q}{Q_0}} \tag{1.15}$$

where i_a (t) is the current flowing through the spring column, u_a (t) - the spring voltage, Q_0 - the amount of heat initially existing in the spring column:

$$Q_0 = \tau \cdot p_0 \tag{1.16}$$

τ - thermal time constant of the electric arc p_0 - the power given by the arc column to the environment, *Q (t)* - the amount of heat accumulated in the arc column:

$$Q(t) = \int_0^t (u_a \cdot i_a - p_0)dt \tag{1.17}$$

It is noted that in order to describe the behavior of the long electric arc, according to Cassie's hypothesis, a shape expression is proposed for the conductance G_a (t).:

$$G_a(t) = k(Q_0 - p_0 \cdot t) \tag{1.18}$$

where $G_a(\tau) = 0, \tau = \frac{Q_0}{p_0}$,

Considering the equation

$$G_a(t) = \frac{i_a(t)}{u_a(t)} = k \cdot e^{\frac{Q}{Q_0}} \tag{1.19}$$

and accepting Mayr's hypothesis, by applying logarithms is obtained:

$$\ln i_a(t) - \ln u_a(t) = \ln k + \frac{Q}{Q_0} \tag{1.20}$$

So after a derivation, Mayr's equation for the long electric arc is written:

$$\frac{1}{i_a} \cdot \frac{di_a}{dt} - \frac{1}{u_a} \cdot \frac{du_a}{dt} = \frac{u_a i_a - p_0}{Q_0} \tag{1.21}$$

By integrating this differential equation we can find the shape of the dynamic characteristic of the alternating current electric arc, for high values of the arc current, so for small values of the current pause, when the relation is valid, [11], [16]:

$$i_a(t) = I \cdot \sin \omega \cdot t \tag{1.22}$$

we obtain the nonlinear first order differential equation of the Bernoulli type which defines the variation as a function of time of the arc voltage, u_a(t):

$$\frac{du_a}{dt} - (\frac{1}{\tau} + \omega \cdot \cot \omega \cdot t) \cdot u_a + \frac{I \cdot \sin \omega t}{\tau p_0} \cdot u_a^2 = 0 \tag{1.23}$$

which turns into a first-order linear differential equation using substitution:

$$u_a = \frac{1}{z}, \frac{dz}{dt} + (\frac{1}{\tau} + \omega \cot \omega t) \cdot z = \frac{I \sin \omega t}{\tau p_0} \tag{1.24}$$

with the final shape solution:

$$u_a(t) = \frac{2 \cdot p_0 \cdot \sin \omega \cdot t}{I \cdot \left[1 - \frac{\sin(2 \cdot \omega \cdot t + \varphi)}{\sqrt{1 + 4 \cdot \omega^2 \cdot \tau^2}}\right]}, \varphi = arcctg2 \cdot \omega \cdot \tau \quad (1.25)$$

The evolution over time of the arc voltage, ua (t), is influenced by the values of the product (ω • τ), as can be seen in Figure 1.7.

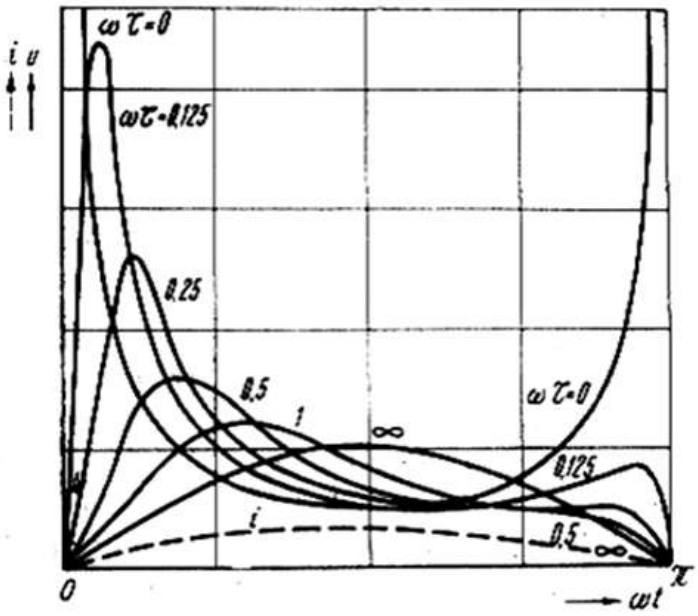

Figura 1.4. Tensiunea arcului electric de c.a, [11]

It is clear that there are three distinct situations:

a) values (ω · τ) = 0, which corresponds to either direct current (ω = 0) or very intense deionizations, for which τ = 0, respectively $p_0 \rightarrow \infty$, which implies high values of the spring priming voltage electric, but also overvoltages to extinguish it;
b) values (ω · τ) comparable to the unit, which highlight a characteristic u_a (t) frequently encountered in the operation of electrical switching devices, showing a priming voltage, U_{am} and a damping voltage, U_{st}, respectively, for each half-period of alternating current;
c) values (ω · τ) → ∞, which correspond to either the free electric arc, $p_0 = 0$, so τ → ∞, or the electric arc that intervenes at high frequencies of the supply voltage, when it behaves practically linear, [11], [16].

CHAPTER 2. Cold plasma discharge power supplies used for various types of reactors. DBD reactor applications

Cold or non-thermal plasma discharges are interesting for example for electrochemical or decontamination applications because they generate active species (electrons, ions, excited particles, photons, etc.), with a very short lifespan, of the order of 10^{-5} dry, but capable of generating metastable radicals (OH- and NO + for example), with a much longer lifespan of $10^{-4} \div 10^{-3}$ sec, which can maintain useful electrochemical reactions, which is not the case with plasma thermal, usable only if thermal effects are exploited, [17], [18].

The main types of electric shocks, commonly called cold plasma due to the low temperature of the gas inside them, are the following:

Corona electric discharge;

luminescent electric discharge, respectively "glow discharge";

GlidArc electric discharge, [17], [18], [19].

2.1. Reactor electrochimic de tip DBD

When the gas penetrates the space between the electrodes, the dielectric prevents the transition to an arc-type discharge. Although uniform spatial unloading in DBD can be accomplished under certain conditions, filament unloading will develop in most circumstances. The filaments are not only spread on the surface, but also appear for a long time. An example: if DBD is driven by a sinusoidal external voltage at a frequency of 100 kHz, the filaments will ignite for a period of about 3 μs in each half-cycle, in successive different stages of external voltage, [21].

DBD discharges are obtained by separating two metal electrodes, which can have different shapes, plane - plane or wire - cylinder, connected to a high voltage source, they are manifested through a layer, or possibly two layers of dielectric material (glass, ceramic, teflon), [17], [23].

Typical electrode configurations of flat and cylindrical dielectric barrier discharges are given in Figure 2.1.

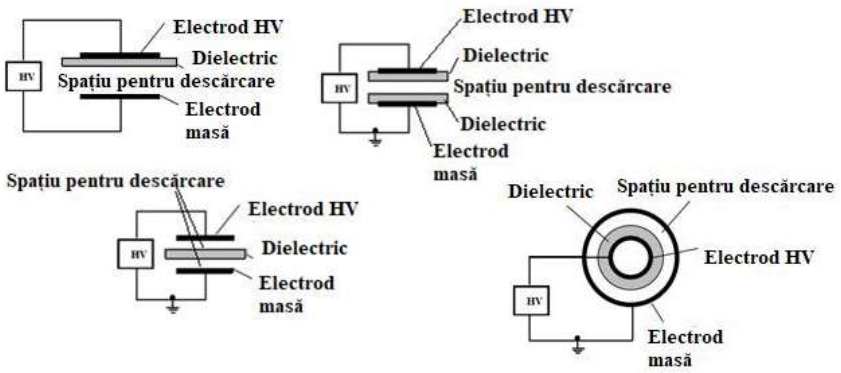

Figure 2.1. Types of DBD reactors, [9]

DBDs are characterized by the presence of one or more insulating layers in the current path between the metal electrodes, in addition to the gap represented by the discharge space, [9].

2.2. Glid Arc electrochemical reactor

The simplified principle diagram of a GlidArc type cold plasma electrochemical reactor is shown in Figure 2.2. It comprises an electrical insulating chamber, usually cylindrical, initially used for the depollution of gases in order to treat a volume as large as possible, [7], [25], [26], [27].

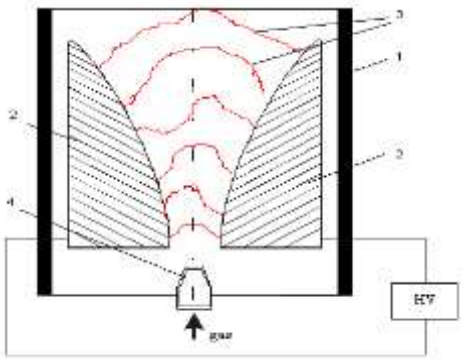

Figure 2.2. GlidArc type electrochemical reactor, [7]

1 - electrical insulated enclosure,
2 - divergent metal electrodes,
3 – electric discharge,
4 - Injection gas nozzle

By connecting the high voltage (HV) source to the metal electrodes, an electric discharge is initiated between them, in the base area, characterized by the minimum bypass distance, discharge that moves on the electrodes, under the action of blowing gas but also forces contour electrodynamics, as well as the upward effect of hot gases in the discharge area, [20], [27], [28]. The blowing gas can be air, nitrogen, oxygen, inert gas, etc, depending on the desired application. The relative displacement speed of the discharge compared to that of the blowing gas is usually 2-4 m / s, [20], [27].

CHAPTER 3. Influence of electrical parameters of power supplies on cold plasma discharge applications

This chapter presents the results obtained with power supplies that are used in obtaining cold plasma in the laboratory. The reactors used are Glid Arc, plasma mini torch and Gliding Spark. In order to observe the influence of electrical parameters, various cold plasma treatments were performed on distilled water under different conditions.

3.1. Experimental power supplies used to produce cold plasma discharges

This subchapter presents the limitations and characteristics of experimentally used power supplies. A transformer built specifically for such applications was most commonly used, with pulsed power supplies being introduced later. For these applications, in addition to the lifting transformer, special construction, 2 pulse power supplies were used, one built with the AT89S52 microcontroller, [65], and the other built with the βAA145 integrated circuit, [66] .

3.1.1. Power supply with TRAF from the network

The 230V / 50Hz mains supply is connected to the mains of a special construction high voltage transformer, such as AUPEM SEFLI AC 10 kV / 150 mA / 50 Hz, which ensures the limitation of the discharge current by its internal impedance. At the output, the transformer offers 10,000 V as a standby voltage, [17].

The diagram for this source, which usually supplies a classic Glid Arc reactor, is shown in Figure 3.1.

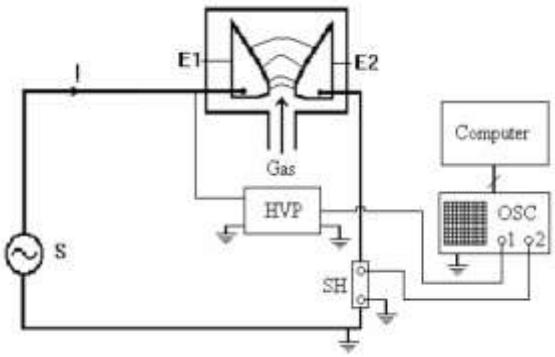

Figure 3.1. Diagram of the connection of a cold plasma reactor to a high-voltage transformer connected to the grid, [17]

No additional current limiting component is required for this application, although energy efficiency is very low (approximately 16%), [17].

3.1.2. βAA 145 power supply

The following power supply is a pulse source built on the βAA145 integrated circuit. This power supply can generate pulses at a maximum frequency of 20 kHz, but the used induction coil transformer does not operate at more than 250 Hz without saturation, [67].

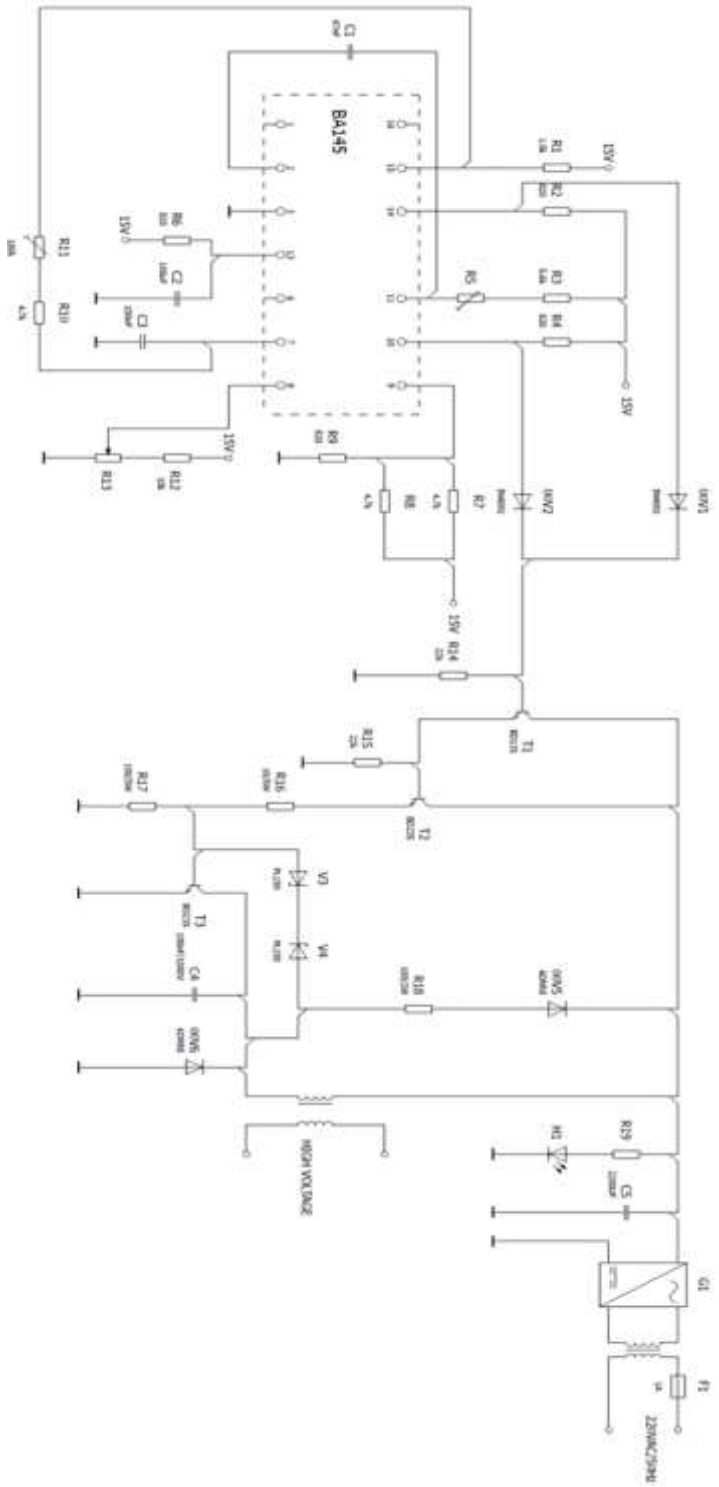

Figure 3.2. Diagram of the power supply built with the help of the integrated βA145, [17]

The pulse width is adjusted by potentiometer R11, resistor R10 and capacitor C3, and this can be adjusted between 0-70% of the duration of a period, Figure 3.2, [67].

The control circuit is supplied with a double stabilized DC voltage source, + 15V, -15V. The power supply is supplied from the mains by means of a separation transformer, rectified and filtered by means of capacitor C5, or from the same stabilized source as the control part.

For the high voltage circuit, the control is given to the transistor T3 connected to the high transformer primary by means of a Darlington type assembly consisting of transistors T1 and T2, controlled in turn from pins 10 and 14 of the integrated circuit, and the reference voltage is found on pin 15, [17] .

The βA145 power supply operates in conjunction with a car coil originally used on OLTCIT vehicles, Figure 3.3. This coil usually supports frequencies on the order of 100 - 200 Hz.

3.1.3. Power supply with AT89S52

The next power supply shown is a pulsed one built around the AT89S52 microcontroller. This source operates at 100Hz due to the high voltage transformer limitation, [17], [18].

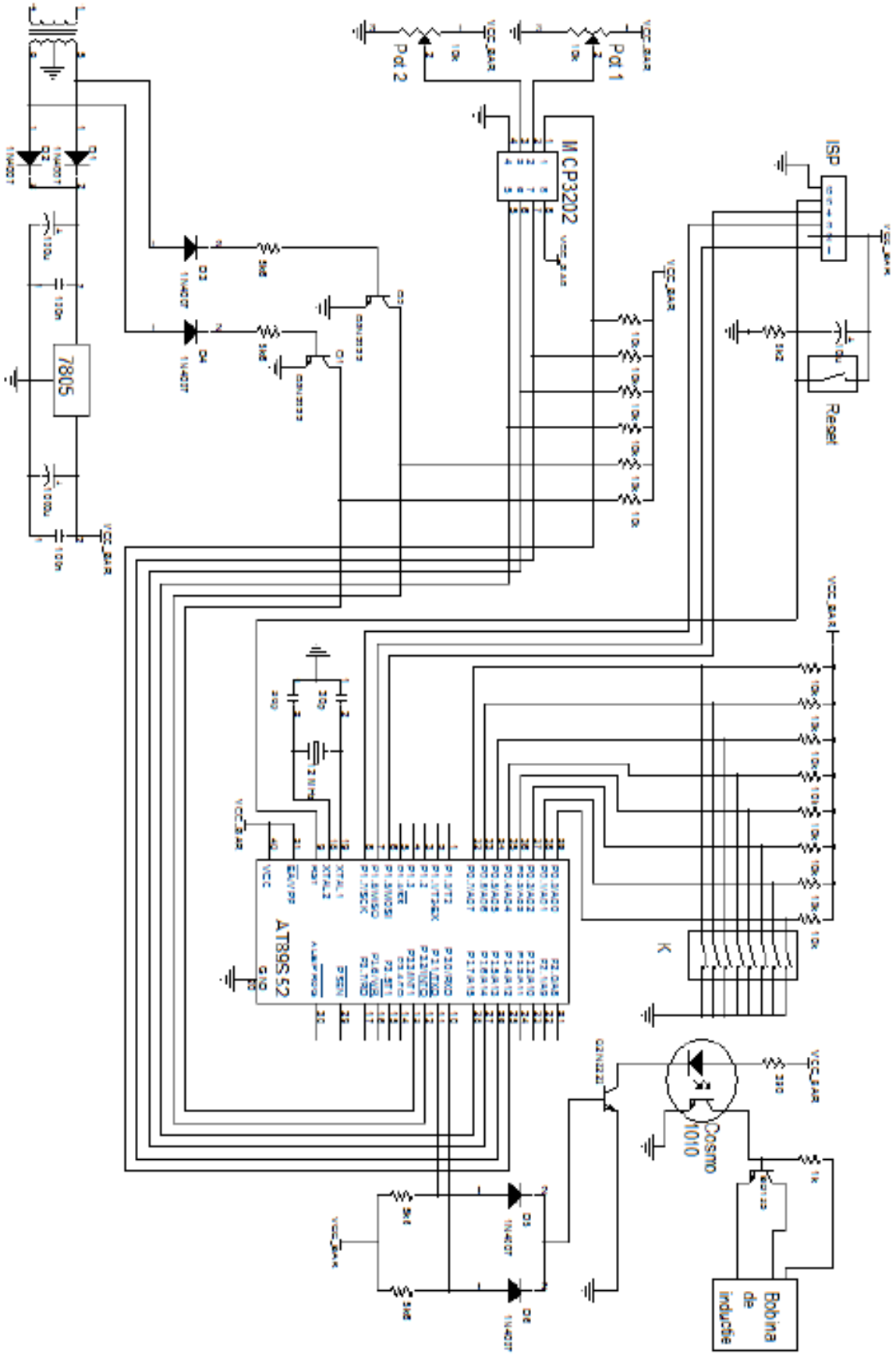

Figure 3.3. Diagram of the power supply built with the ATS89S52 microcontroller, [17], [18]

The source built around the AT89S52 is designed to produce spark-type discharges. The LM7805 integrated circuit was used to supply the stabilized voltage circuit (pins 12,13). The MCP3202 integrated circuit used to convert analog signals from Pot1 and Pot2 potentiometers to digital signals uses the SPI communication protocol with the microcontroller, to read the voltage values on 2 potentiometers, considered as input variables and to ensure their conversion into pulse trains. 2 corresponding microcontroller outputs, [17], [18].

To control the power transistor, the microcontroller outputs on pins 10, 11 are connected to an optocoupler which in turn forms a Darlington-type circuit with the power transistor. The circuit is used in conjunction with a TV or monitor line switch shown in Figures 3.5 and 3.6.

3.1.4. High voltage power supply at 30 kHz, AC voltage

This power supply used is shown in the Figure below (Figure 3.4). As can be seen, it was intended for the production of electric discharges in quartz tubes containing different types of gases.

Figura 3.4. Specificația sursei de 30 kHz

This alternating current source operates at 30 kHz and has an output voltage of 8000V. Inside this source is a modulator / frequency converter that raises its value from 50 Hz to 30 kHz.

3.2. Particular construction types of reactors used experimentally

Due to the exploration of non-thermal plasma in various applications, this technology is being used more and more due to the advantages that include increased treatment efficiency, low cost and ease of use.

3.2.1. GlidArc classic

For plasma treatments, one of the reactors used is GlidArc Classic or GlidArc I, as previously named. This is shown in Figure 3.5. The main disadvantage of this reactor is that the treatment applied has a dissipative nature.

Figure 3.5. GlidArc Reactor, [67], [70]

In order to increase the electrochemical efficiency, the use of these reactors has changed from two metal electrode assemblies to three electrode (or multiple 3 electrode) assemblies, preferring the volume manifestation of useful electric discharge, both for single-phase power supplies, especially for three-phase power supplies, [67].

3.2.2. Plasma Mini Torch

Another type of reactor used is the plasma minitorchch, Figure 3.6. This reactor uses a stream of air that passes through a metal grid with several holes. The inner part has a frustoconical, nozzle shape, and the discharge is initiated between the central electrode, in the shape of a rod, and the outer one in the truncated cone shape.

Figura 3.6. Reactor tip torță de plasmă

This minitorchch-concentrate concentrates the plasma flow through a nozzle.

3.2.3. Gliding Spark reactor

This type of reactor is made of a metal box, with two airflow connections and a classic car spark plug modified as the main enclosure.

Figure 3.7. Gliding-Spark plasma reactor (Nox Box)

The discharge chamber has a much smaller volume than the previous reactors. The center electrode of the spark plug is fed to the high voltage potential, and the metal housing of the reactor is connected to the reference potential. The airflow is introduced through a connection and the plasma outlet is made through the second connection [71].

3.3. Influence of electrical parameters specific to cold plasma reactors

This subchapter presents the graphs of electrical parameters, electric discharge current, discharge resistance, useful power and specific energy, as a function of time. These parameters were collected under the following conditions: 2 records, the voltage was obtained by dividing by 1000 with the help of a high voltage probe, and the current by multiplying by 5 and dividing by 1.6, as a result of using a shunt. The useful power, the discharge resistance and the specific energy were obtained by calculation from the measured parameters. The first recording was made at a flow rate of 5 l / min and the second at 15 l / min. The distance measured between the electrodes was 2mm.

Considering a linear approximation of the combination and recombination phenomena, the discharge volume evolves linearly according to the values of current and voltage. Thus, the volume for the discharge of the Glid Arc reactor used as 5484 mm^3 was measured and calculated, depending on the size of each reactor, for the mini-plasma the volume is 126 mm^3 and for the Gliding Spark reactor the discharge volume is 262 mm^3.

Since the actual discharge depends on parameters such as gas flow rate, inter-electrode lag, arc length and evolution time, the evolution of the discharge is consistent with different voltage variations and flow rates.

3.3.1. Glid Arc reactor specific electrical parameters

Figures 3.8, 3.9, 3.10 and 3.11 show the evolution of the electrical parameters of the discharge over time using the classic GlidArc reactor with an air flow of 5 l / min, connected to the high voltage transformer type AUPEM (230V / 50Hz - 10000V / 50Hz).

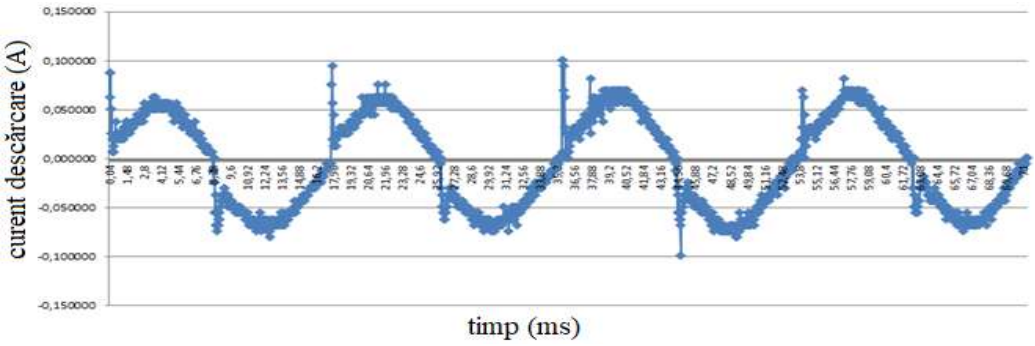

Figure 3.8. The evolution of the discharge current over time for a GlidArc reactor connected to the AUPEM transformer and an air flow of 5 l / min, [70]

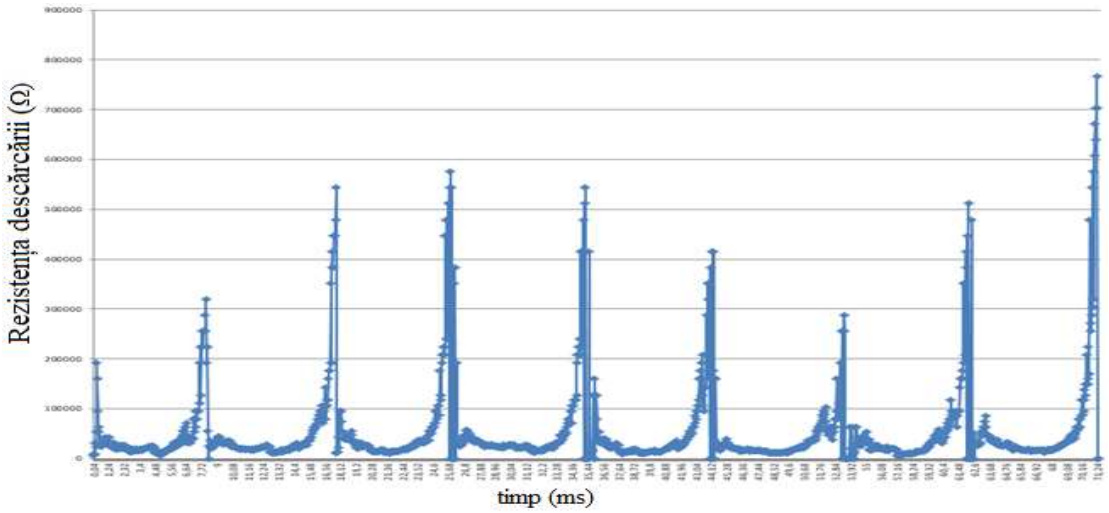

Figure 3.9. The evolution of the discharge resistance over time for a GlidArc reactor connected to the AUPEM transformer and an air flow of 5 l / min, [70]

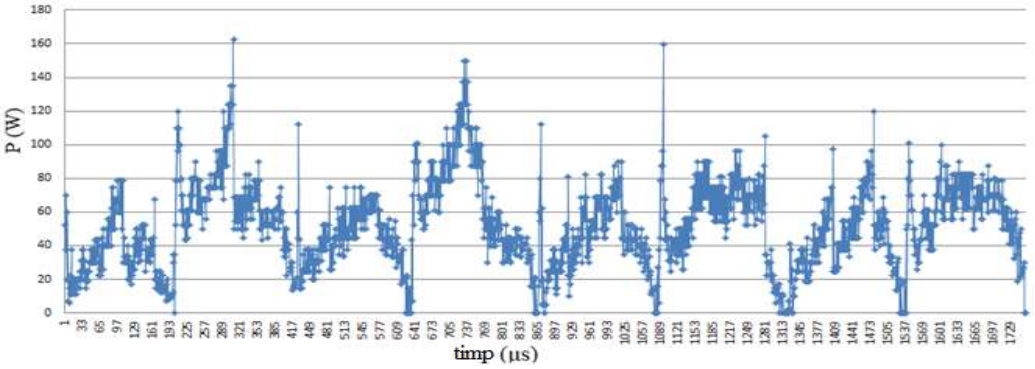

Figure 3.10. The evolution over time of the electric power for the GlidArc reactor, air flow of 5 l / min, [67]

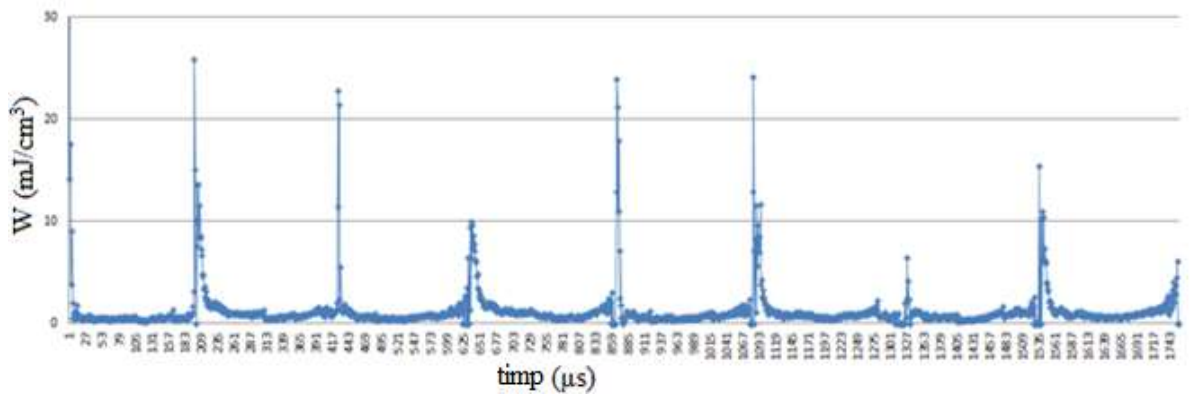

Figure 3.11. The evolution over time of the specific energy for the GlidArc reactor, air flow of 5 l / min, [67]

The figures shown show that the evolution of the current follows the sinusoid (given by the frequency and voltage of the network) and shows peak values of the order of milliamperes.

3.3.2. Minimum reactor specific parameters

Figures 3.12, 3.13, 3.14 and 3.15 show the graphs of the electrical parameters useful discharge power, specific energy, electric discharge current and discharge resistance, using the mini-plasma reactor with an air flow of 5 l / min connected to the high transformer AUPEM type voltage (230V / 50Hz - 1000V / 50Hz).

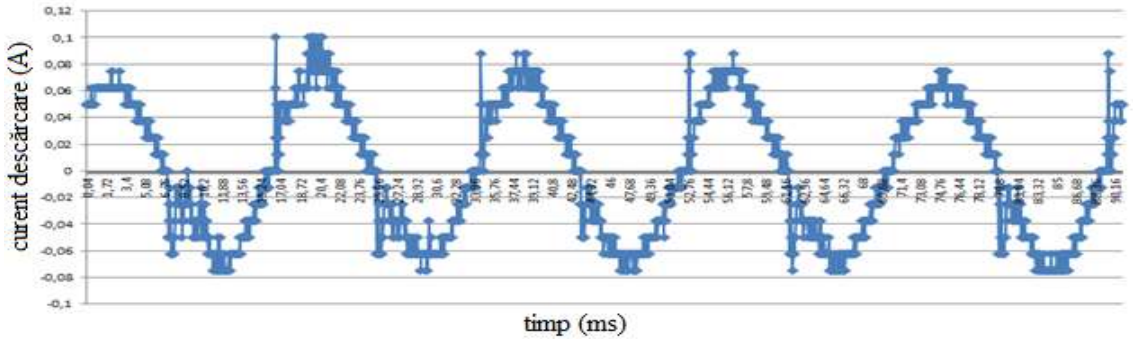

Figure 3.12. Over time evolution of the discharge current for the mini torch reactor, connected to the AUPEM transformer, for an air flow of 5 l / min, [70]

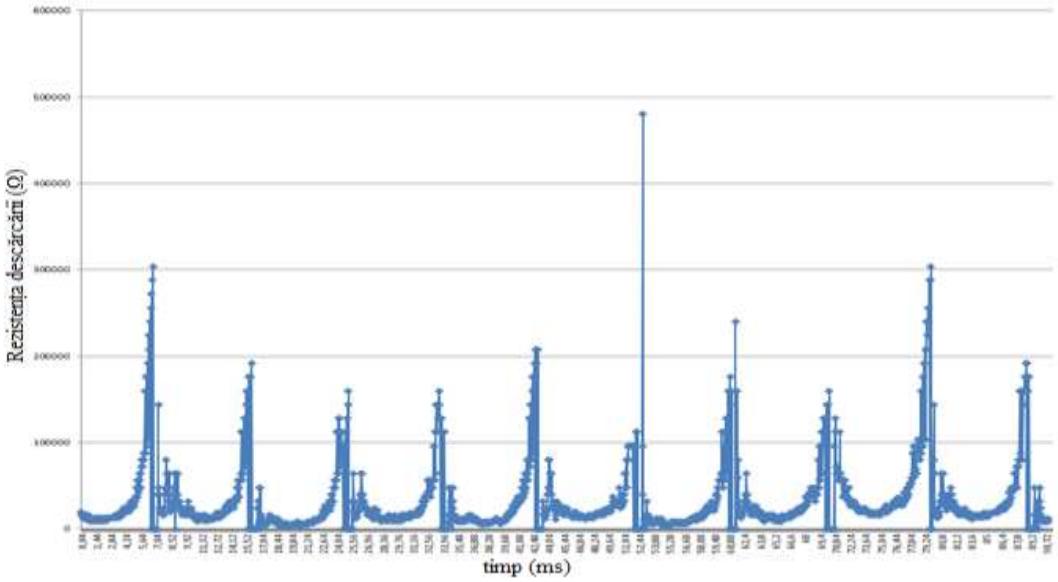

Figure 3.13. The evolution of the discharge resistance over time for the mini torch reactor, connected to the AUPEM transformer, for an air flow of 5 l / min, [70]

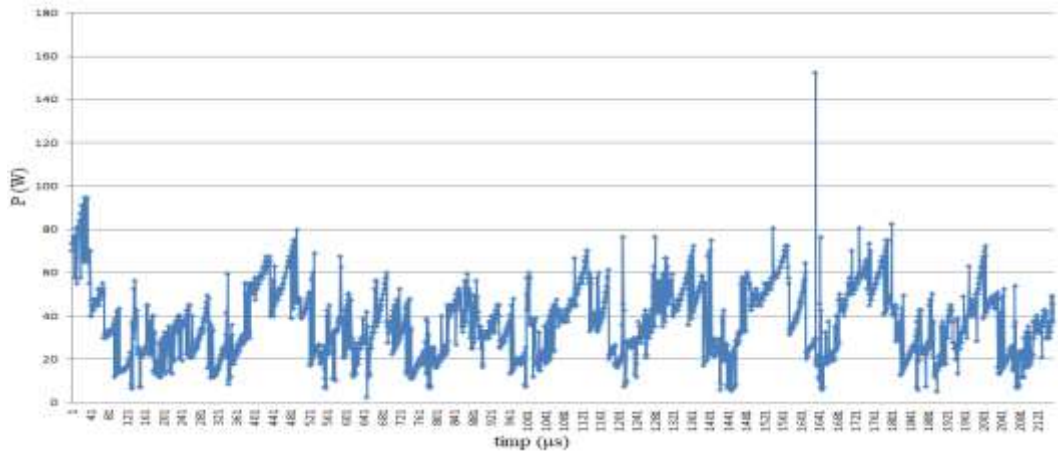

Figure 3.14. The evolution in time of the electric power for the mini torch reactor, air flow of 5 l / min, [67]

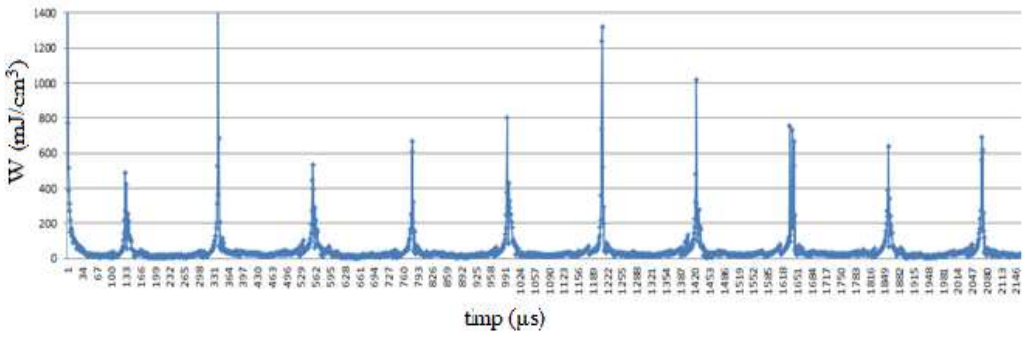

Figure 3.15. The evolution in time of the specific energy for the mini torch reactor, air flow of 5 l / min, [67]

The figures shown above show the evolution of current, discharge resistance, electrical power and specific energy.

3.3.3. Gliding Spark reactor specific parameters

Figures 3.16, 3.17, 3.18 and 3.19 show the graphs of the electrical parameters useful power, specific energy, electric discharge current and discharge resistance, using the Gliding Spark reactor (also called NOx Box) with a connected air flow of 5 l / min to the AUPEM type high voltage transformer (230V / 50Hz - 1000V / 50Hz).

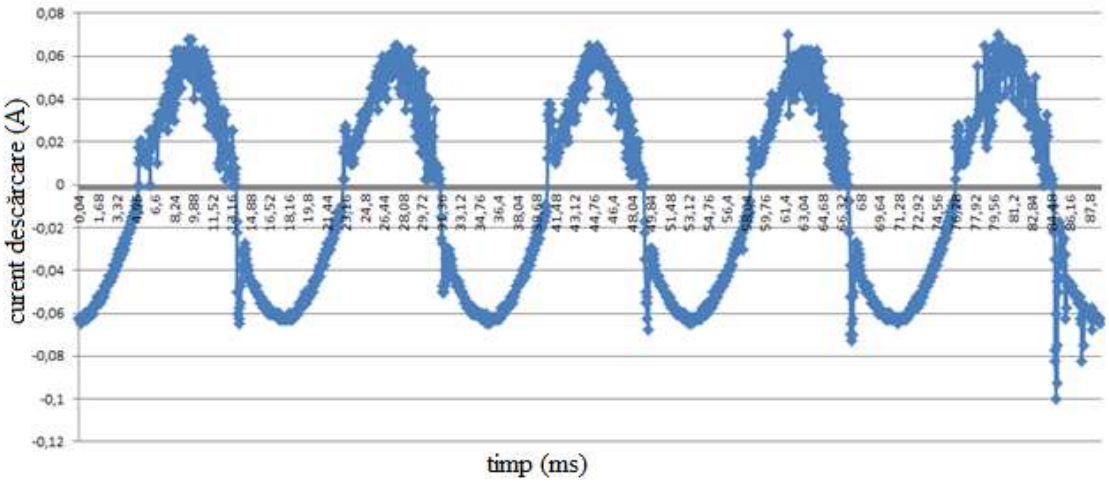

Figure 3.16. Evolution of the discharge current over time for Gliding Spark, air flow of 5 l / min, [70]

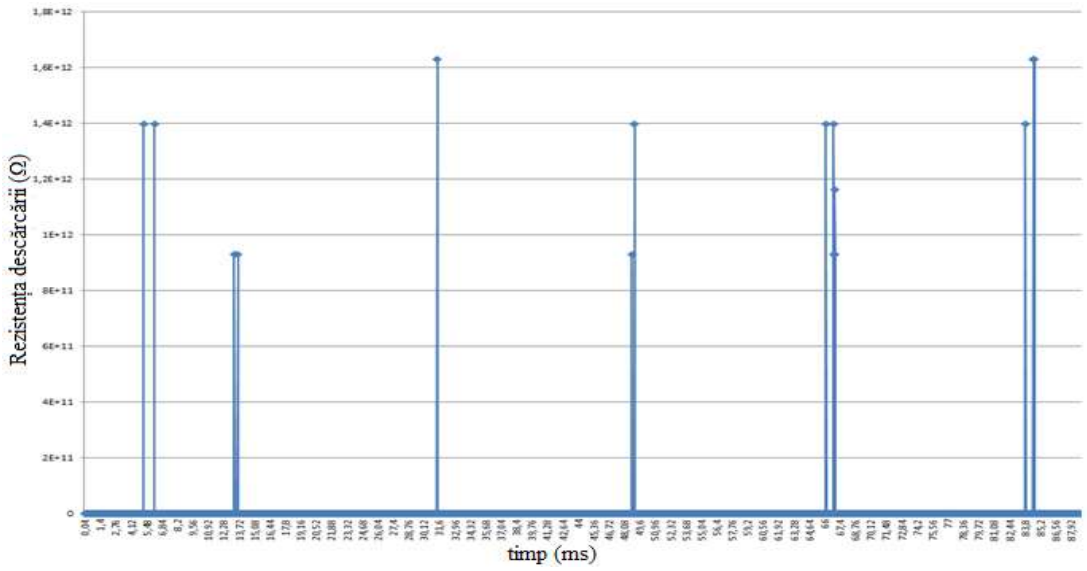

Figure 3.17. The evolution of the discharge resistance over time for Gliding Spark, air flow of 5 l / min, [70]

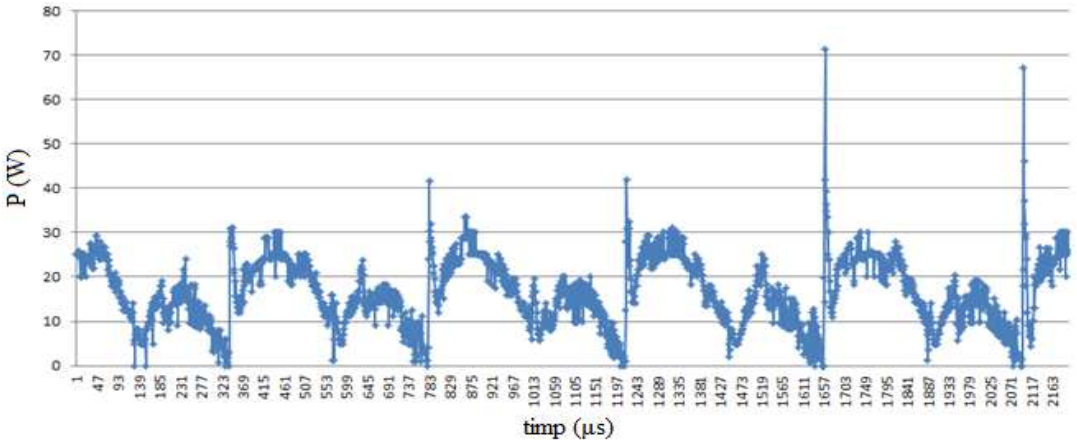

Figure 3.18. Evolution over time of the useful electric power for the Gliding Spark reactor, air flow of 5 l / min, [67]

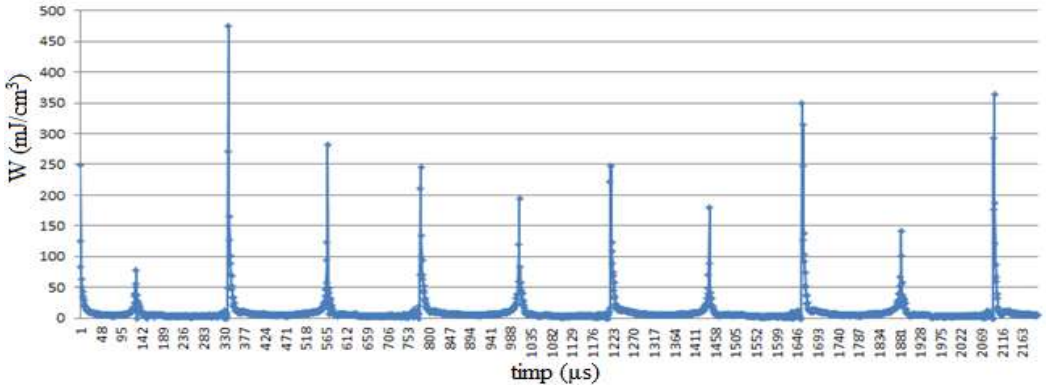

Figure 3.19. The evolution over time of the specific energy for the Gliding Spark reactor, air flow of 5 l / min, [67]

The current shows an almost sinusoidal evolution and unlike the previous cases there are no current peaks.

Parametric study shows that, from a qualitative point of view, the increase in current increases the size of the electrode hotspot.

Compared to the approximation used, the results are strongly nonlinear, as expected, given Paschen's law and electron-ion recombination.

The useful electric power values are the highest in the case of the GlidArc reactor, followed by the minitorchch reactor and the Gliding Spark reactor.

3.4. Influence of electrical parameters of power supplies on electrical parameters of substances treated with particular cold plasma reactors

The experimental results of this subchapter were obtained from the plasma distillation activation treatment obtained using the power supplies and reactors presented in subchapters 3.1 and 3.2. The first step in the analysis of distilled water was to establish a reference by collecting data from an untreated sample. The FISHER SCIENTIFIC XL600 analyzer was used to measure the pH and redox potential of the solution.

The first set of samples collected is shown in Figures 3.20 and 3.21. They correspond to untreated samples, to then highlight the effects of plasma treatment using different reactors and power supplies.

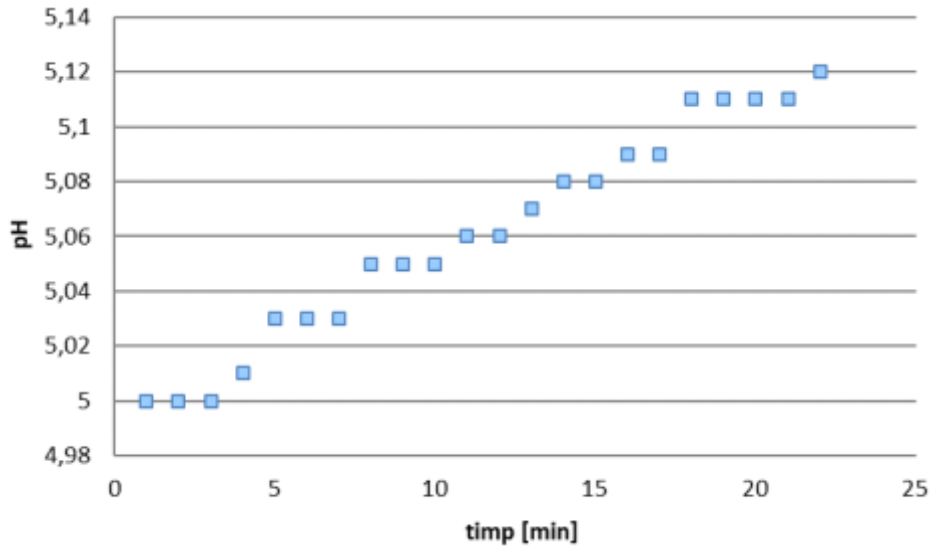

Figure 3.20. PH change over time in the case of an untreated distilled water sample, [70]

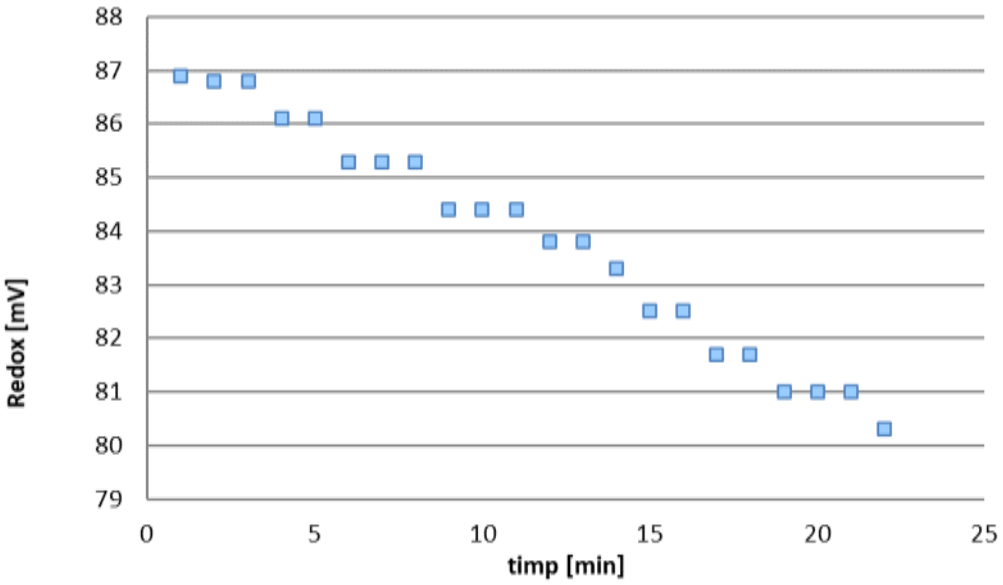

Figure 3.21.Variation of Redox potential over time in the case of an untreated distilled water sample, [67]

As can be seen, the values remain relatively constant, the variations being very small in the case of the decreasing redox reaction, and in the case of the increasing pH variation.

3.4.1. Non-electrical parameters resulting from treatment with the Glid Arc reactor

The following data were obtained under the following experimental conditions: 200 ml of treated distilled water, at a distance of 25 mm between the solution and the electrode end, the reactor used being the classic Glid Arc, and the power supply used being the high voltage AUPEM transformer (230V / 50Hz - 1000V / 50Hz) connected directly to the mains for an airflow of 25l / min, Figure 3.22.

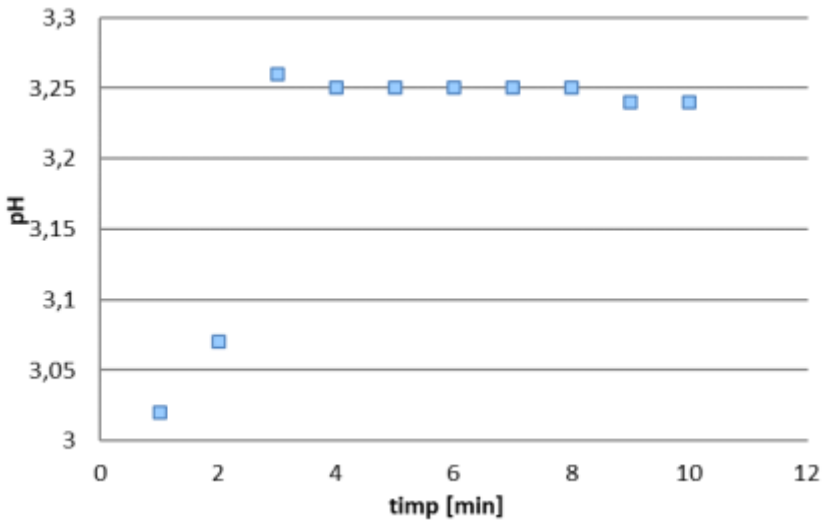

Figure 3.22. PH change over time after cessation of treatment using GlidArc reactor and AUPEM transformer - air flow 25 l / min, [70]

After treatment, the pH parameter decreased from 5-5.12 to 3 - 3.25, remaining relatively constant around this value.

The pH graph, as a function of time, can be seen in Figure 3.23. These parameters were collected under the following conditions: 3 records, 200 ml of treated distilled water, a distance of 25 mm between the end of the electrodes and the solution to be treated. The classic GlidArc reactor was used, the pulse power supply based on the βA145 circuit. The first series of analyzed samples was collected for an air flow of 18 l / min, the second series analyzed for an air flow of 25 l / min and the third series corresponds to an air flow of 32 l / min.

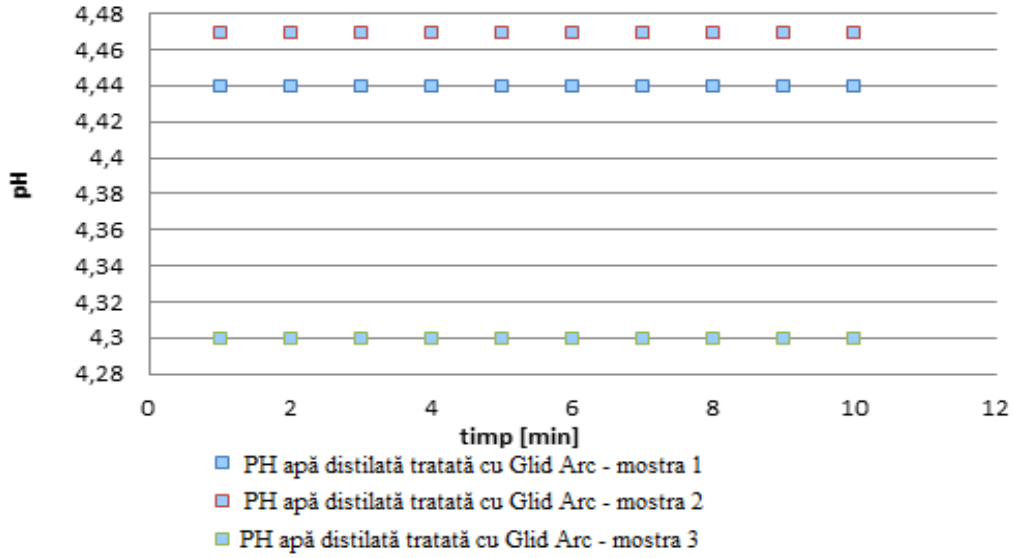

Figure 3.23. Variation of pH over time using GlidArc reactor connected to source with βA145 circuit - air flow for sample 1 - 18 l / min, sample 2 - 25 l / min, sample 3 - 32 l / min, [70]

In this case the pH variation is smaller (compared to the reference considered), the values remaining constant.

Below are the graphs of the non-electrical parameters pH, Figure 3.24, as a function of time, obtained under the following conditions: 3 records, 200 ml of treated distilled water, a distance of 25 mm, the classic GlidArc reactor used, AC power supply of 30 kHz. The first series of samples analyzed was collected for an air flow of 18 l / min, the second series collected for an air flow of 25 l / min and the third series corresponding to an air flow of 32 l / min.

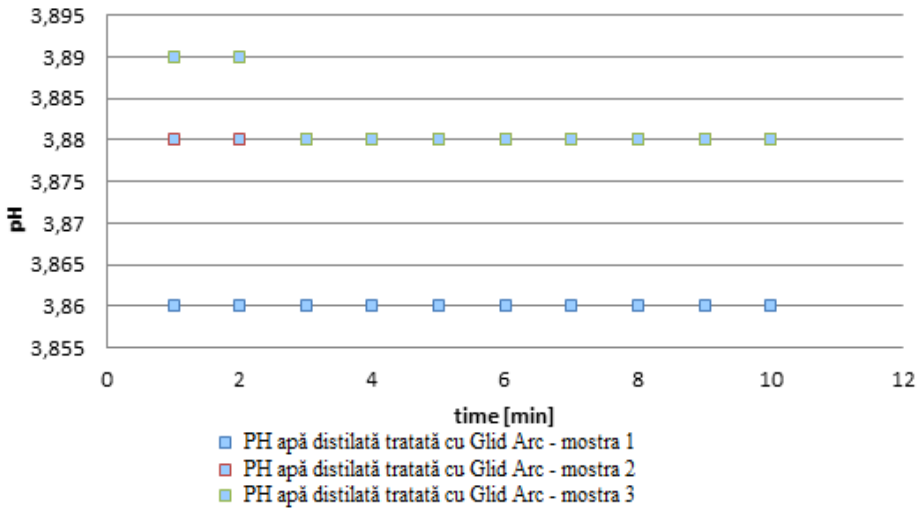

Figure 3.24. Variation of pH over time using GlidArc reactor connected to 30 kHz source - air flow for sample 1 - 18 l / min, sample 2 - 25 l / min and sample 3 - 32 l / min [70]

Following this treatment, it is observed that the 30kHz source is more efficient, the pH values are close to 3.8, the variations being insignificant.

3.4.2. Non-electrical parameters resulting from treatment with the mini-reactor

The following data collected were taken under the following experimental conditions: 200 ml of treated distilled water, at a distance of 25 mm between the solution and the electrode end, the reactor used being the minitorch, and the power supply used was the high voltage transformer AUPEM (230V / 50Hz - 1000V / 50Hz) connected directly to the network, for an air flow of 25l / min.

For treatment with plasma minitorchies, it is observed that the pH value decreases to 3 but gradually increases to 3.27 (Figure 3.25).

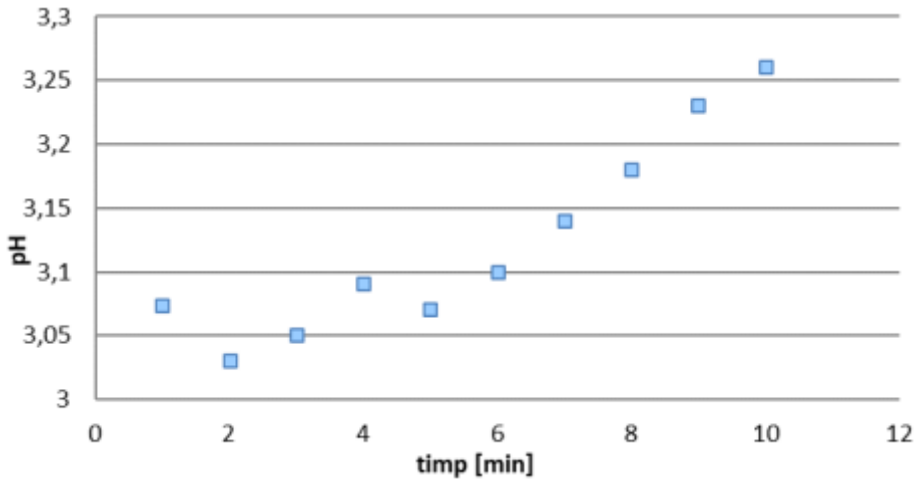

Figure 3.25. PH variation over time using the Plasma mini-flow reactor connected to the AUPEM transformer - air flow 25 l / min, [70]

The values of the non-electrical parameters pH (Figure 3.26), as a function of time, are shown below. These parameters were recorded under the following conditions: 3 records, 200 ml of treated distilled water, distance of 25 mm, mini-reactor, pulse power supply based on the βA145 circuit. The first series of analyzed samples was collected for an air flow of 18 l / min, the second series for an air flow of 25 l / min and the third series for air flow of 32 l / min.

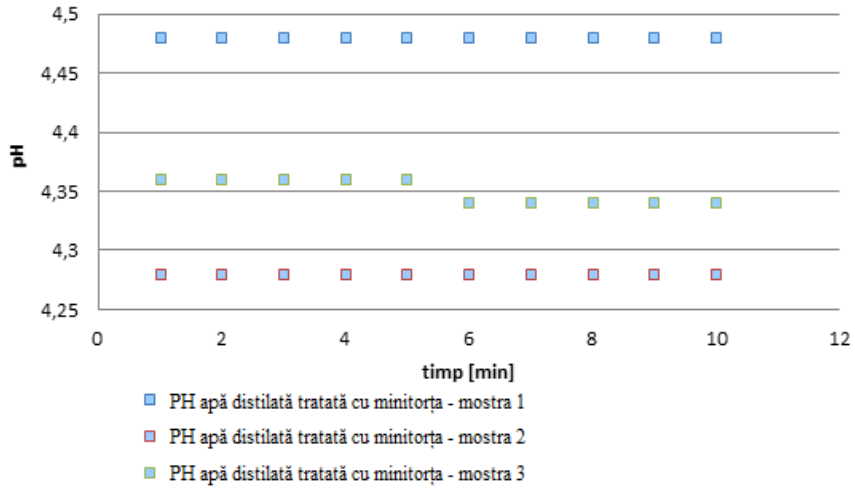

Figure 3.26. Variation of pH over time using Plasma tinplate connected to source with βA145 circuit - air flow for sample 1 - 18 l / min, sample 2 - 25 l / min and sample 3 - 32 l / min, [70]

The pH variation in this case is between 4.3 and 4.48. These values show that the treatment with the mini-plasma reactor is less effective in treating a quantity of liquids than the treatment with Glid Arc.

Further developments can be seen within 12 minutes of stopping plasma pH treatment (Figure 3.27). These were performed under the following conditions: 3 recordings, 200 ml of treated distilled water, distance of 25 mm, the reactor used being the minitorch, the power supply in pulses based on the AT89S52 microcontroller. The first series of data corresponds to an air flow of 18 l / min, the second series to an air flow of 25 l / min and the third series to an air flow of 32 l / min.

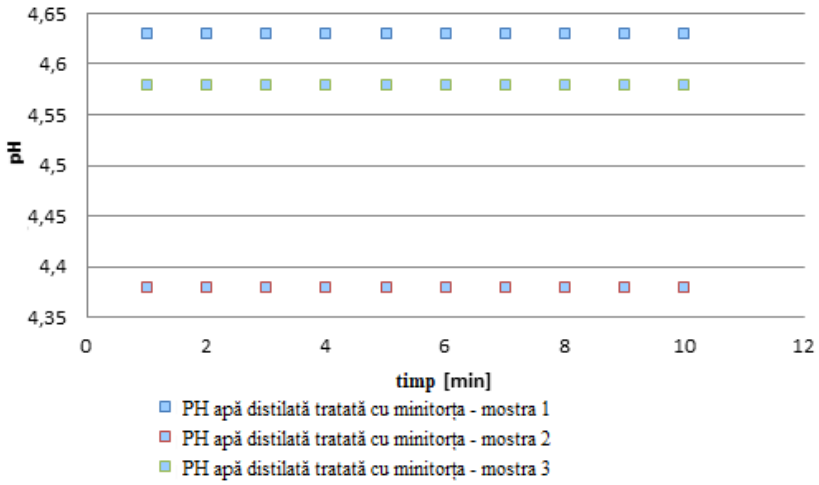

Figure 3.27. Variation of pH over time using the Plasma Minithink connected to the source with the AT89S52 circuit - air flow for sample 1 - 18 l / min, sample 2 - 25 l / min and sample 3 - 32 l / min, [70]

In the case presented, the pH variation between the values 4.38 and 4.63 is observed, the variation being due to the air flow, the results being weaker compared to the previous case.

The following graph of the evolution of pH (Figure 3.28), depending on the time, was obtained under the following conditions: 3 records, 200 ml of treated distilled water, distance of 25 mm, the reactor used being the minitorch, and the power supply the alternating current of 30 kHz. The first row of data corresponds to an air flow of 18 l / min, the second to an air flow of 25 l / min and the third to an air flow of 32 l / min.

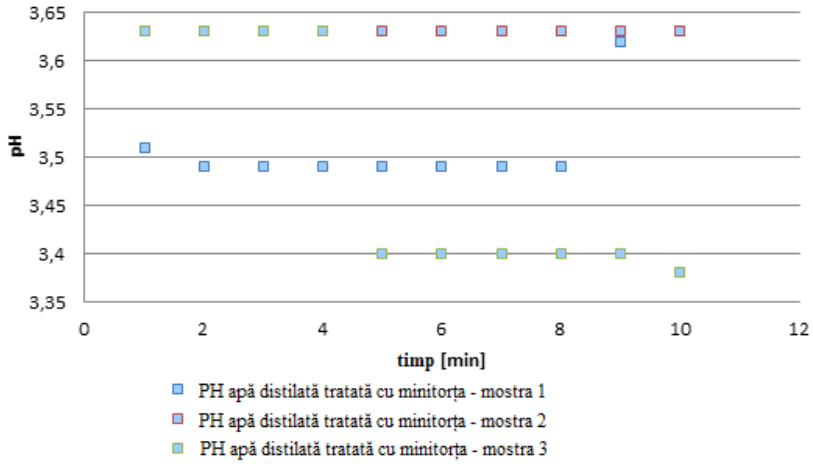

Figure 3.28. Variation of pH over time using 30 kHz Plasma Mini-Connector - airflow for sample 1 - 18 l / min, sample 2 - 25 l / min and sample 3 - 32 l / min, [70]

The graphs show that the pH variation is between 3.4 and 3.63, the values being due to the frequency at which the source operates.

3.4.3. Non-electrical parameters resulting from treatment with the Gliding Spark reactor

The following graphs were drawn from the corresponding experimental conditions: 200 ml of treated distilled water, a distance of 25 mm between the solution and the electrode end, the reactor used being Gliding Spark (NOx Box), and the power supply used the high voltage transformer AUPEM (230V / 50Hz - 1000V / 50Hz), connected directly to the network. The air flow in this case was 25l / min. Thus, Figure 3.29 shows the pH variation.

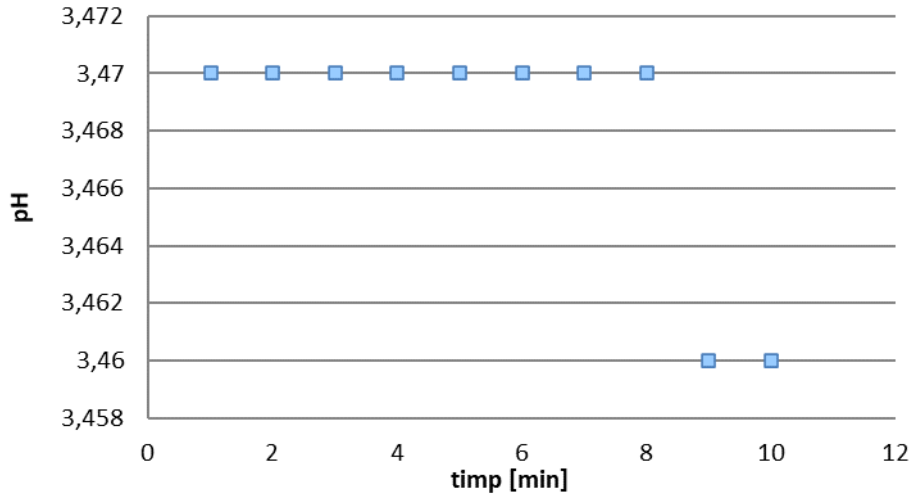

Figure 3.29. PH variation over time using Gliding Spark connected to AUPEM transformer - air flow 25 l / min, [70]

In the case presented, a lower efficiency of this reactor is observed compared to the other two reactors, the pH varying between the values 3.46 and 3.47.

Below are the pH graphs (Figure 3.30), as a variation as a function of time. The registered parameters consist of: 3 series of tests, 200 ml of treated distilled water, distance of 25 mm, the reactor used being Gliding Spark (NOx Box), and the power supply in pulses based on the βA145 circuit. The first series of data corresponds to an air flow of 18 l / min, the second series analyzed to an air flow of 25 l / min and the third series corresponds to an air flow of 32 l / min.

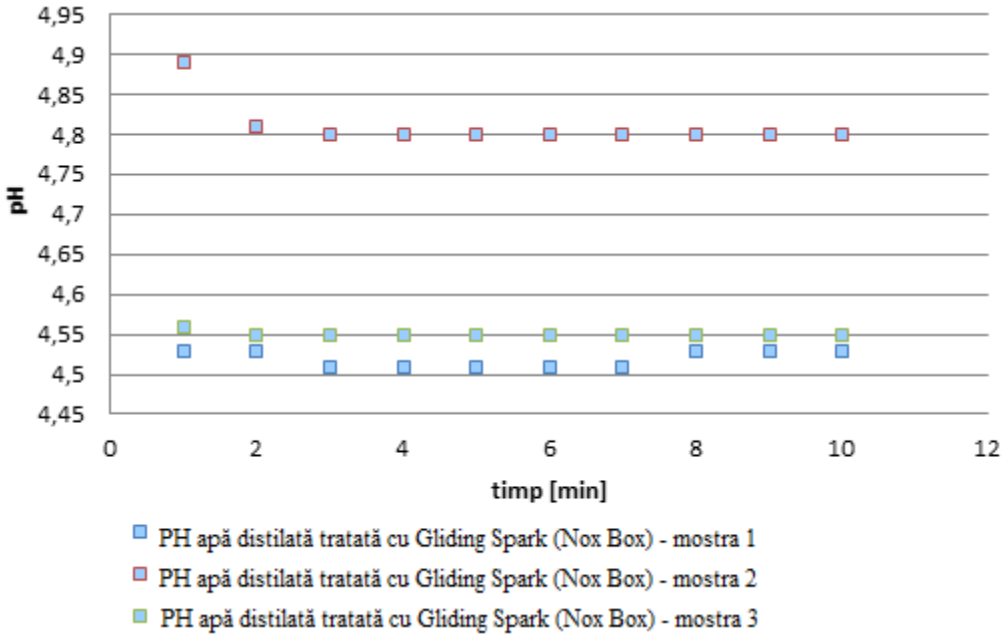

Figure 3.30. PH variation over time using Gliding Spark connected to source with βA145 circuit - air flow for sample 1 - 18 l / min, for sample 2 - 25 l / min and for sample 3 - 32 l / min, [70]

For this case, the pH variation is very small, the values depending a lot on the air flow and being between 4.5 and 4.9.

The time evolutions of the pH parameters are presented below in Figure 3.31, being stored in the following conditions: 3 records, 200 ml of treated distilled water, distance of 25 mm, the reactor used being Gliding Spark (Nox Box), impulse power supply based on the AT89S52 microcontroller. The first series of data corresponds to an air flow of 18 l / min, the second series corresponds to an air flow of 25 l / min and the third series corresponds to an air flow of 32 l / min.

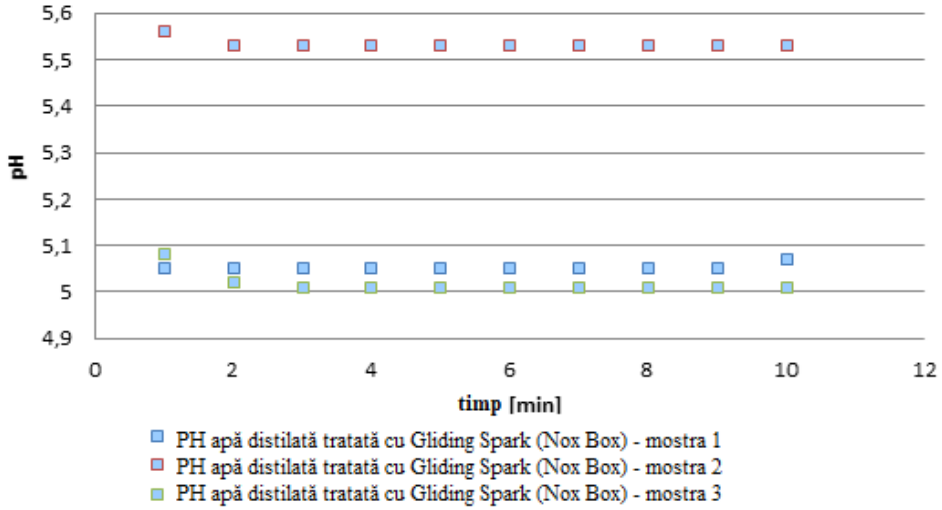

Figure 3.31. PH variation over time using Gliding Spark connected to the source with AT89S52 - air flow for sample 1 - 18 l / min, for sample 2 - 25 l / min and for sample 3 - 32 l / min, [70]

For this case the treatment is inefficient, the pH values being almost identical to the value of untreated distilled water.

Below are the pH values (Figure 3.32), as a variation as a function of time. These parameters were collected under the following conditions: 3 records, 200 ml of treated distilled water at a distance of 25 mm, the reactor used being Gliding Spark (Nox Box), 30 kHz AC power supply, first series of samples analyzed was collected for an air flow of 18 l / min, the second series analyzed was collected for an air flow of 25 l / min and the third series corresponds to an air flow of 32 l / min.

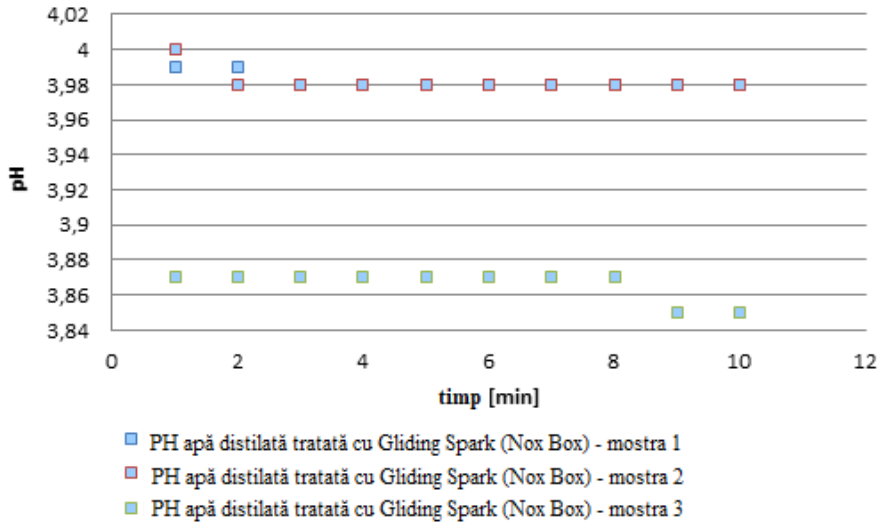

Figure 3.32. Variation of pH over time using the Gliding Spark reactor connected to the 30 kHz source - air flow for sample 1 - 18 l / min, for sample 2 - 25 l / min and for sample 3 - 32 l / min, [70]

The value of the 30kHz frequency helps a lot the treatment presented in these figures, the pH values being between 3.87 and 4.

In addition to the construction of the reactor, a very important role in the efficiency of the treatment with cold plasma discharge is also provided by the power supplies.

The calculation of the discharge resistance for the approximate volume of plasma showed that a lot of active species are dispersed in too large a volume for the conventional GlidArc reactor, so the payload is not used efficiently.

Analyzing the influence of the electrical parameters of different power sources used together with different types of reactors, data were extracted with the electrical parameters specific to the reactors correlated with the non-electrical parameters, namely the pH.

For pH measurements, the most stable results were obtained when using the classic GlidArc reactor due to the plasma treatment surface, using the AUPEM type transformer. In most experiments, the pH values were constant during the 10-minute measurement.

All tests performed using the AUPEM transformer as a power supply have yielded satisfactory results, but at the same time it must be taken into account that similar results were obtained at lower powers and higher frequencies. Thus, frequency is an important factor in the treatment of cold plasma.

CHAPTER 4. Development and modeling of high voltage power supplies designed for DBD type discharges. Experimentally used reactors

This chapter presents and analyzes the simulation of some power supplies. The analysis consists of visualizing the control signals, comparing the power circuit for the analyzed circuits and also comparing it with a connection to a resistor and a connection to the discharge itself. The power supplies have a maximum frequency of 60 kHz due to the limitations of the high voltage transformer.

4.1. Emulation by means of an equivalent circuit of cold plasma discharges

In order to optimize the non-thermal plasma treatment for different applications, the parameters of the electric discharges that produce the plasma must be taken into account.

A download simulation circuit is used to test the download connection. This circuit is shown in Figure 4.1. The circuit is designed using capacitors to simulate the collection of energy before discharge and a resistor that simulates the discharge resistance itself. The relay is used to reproduce the charge of the capacitor and its discharge on the resistor, thus equivalent to the electric discharge between the electrodes.

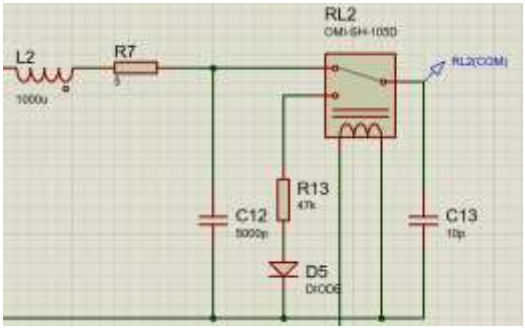

Figure 4.1. Circuit used to simulate cold plasma electric discharge, [72]

The value of the characteristic voltage parameters corresponding to the capacity is entered in a wiring diagram of a classical model. The simulation results are taken into account with a correlation with the electrical parameters of a pulse voltage source.

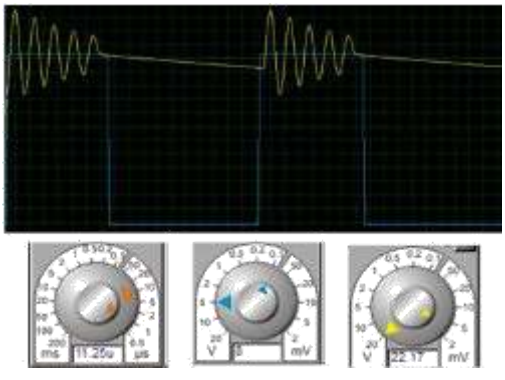

Figure 4.2. Results of the equivalent download circuit simulation, [73]

The behavior of the discharge at the moment of initiation is equivalent to that of a D diode placed on the same circuit branch with a low value resistance, which is the element of dissipation of the accumulated energy, equivalent to the production of an electric discharge of the spark type.

The electrical circuit used to simulate the evolution of the discharge voltage allows a single modification of the circuit structure for the study of the transient priming regime produced.

Oscillations at this frequency occur during non-zero values of the spark discharge current.

4.2. Simulation of the power supply built with the integrated circuit TL494

The circuit built around the integrated TL494 is versatile and can control a half bridge or full bridge bridge of MOSFETs or IGBTs through a gate control transformer (GDT). This should make a driver that is able to control the flyback transformers found in CRT TVs and computer monitors, [72].

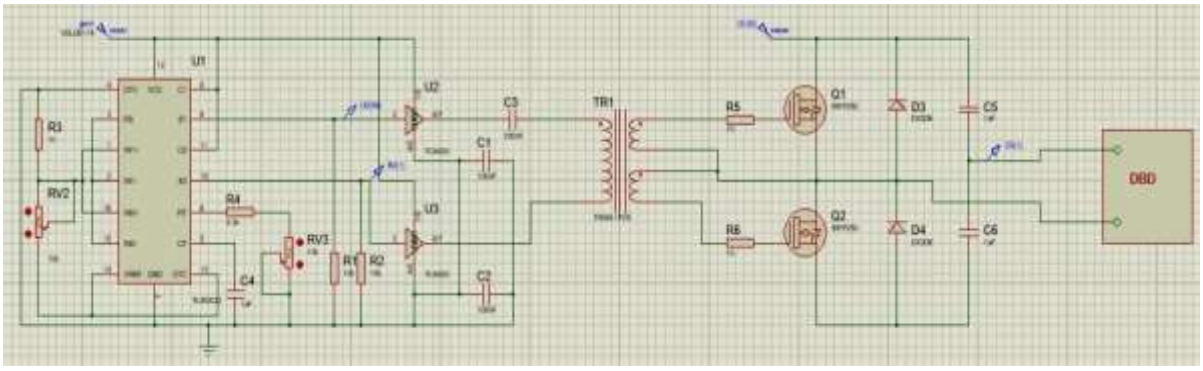

Figure 4.3. Complete diagram of the power supply with the TL494 circuit,[72]

The power supply shown is built around the TL494 integrated circuit. This source offers a variable frequency between 20 and 90 kHz with a variation of the filling factor between 0% and 50%, [72].

The pulse width is manually controlled for the tests that have been performed.

The output control on pin 13 is set to a 5 volt reference voltage on pin 14, which causes the two output transistors to operate in push-pull mode, which will be used to drive each of their ICs. reverse MOSFET driver, [72].

To adjust the operating cycle, the error amplifier was configured as a voltage monitor, the feedback from the operational amplifier being connected to the input, so the output voltage was just below the value of the input voltage. With a potentiometer and a resistor, the input voltage can be varied from 0.5 V to 4.76 V, this voltage being sufficient to adjust the operating cycle from 0 to 43%, [72].

The simulation results for the power supply are illustrated in Figure 4.4.

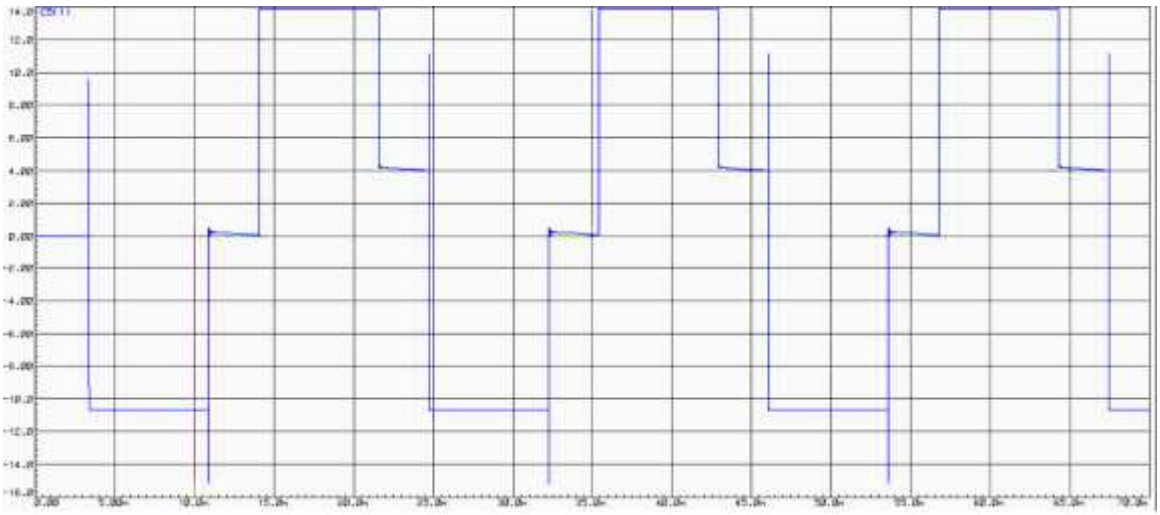

Figure 4.4. The result of simulating the power supply with the TL494 circuit, [74]

The discharges that take place are also based on the oscillations provided by the capacitors C5 and C6 respectively and the primary winding of the inductor (inside the block called DBD).

This universal inverter makes it possible to adjust the output voltage and current. This helps make a flyback driver more robust than other simple drivers with just one transistor, as it implements its own control, MOSFET driver, and half-bridge topology.

4.3. Simulation of the power supply built with the integrated SG2525

The SG2525 integrated circuit is used in the standard PWM generator / oscillator connection where the oscillation frequency is determined by C2, R7 and RV2. The RV2 potentiometer can be adjusted to obtain exact frequencies according to the required application specifications. The scheme is shown in Figure 4.5.

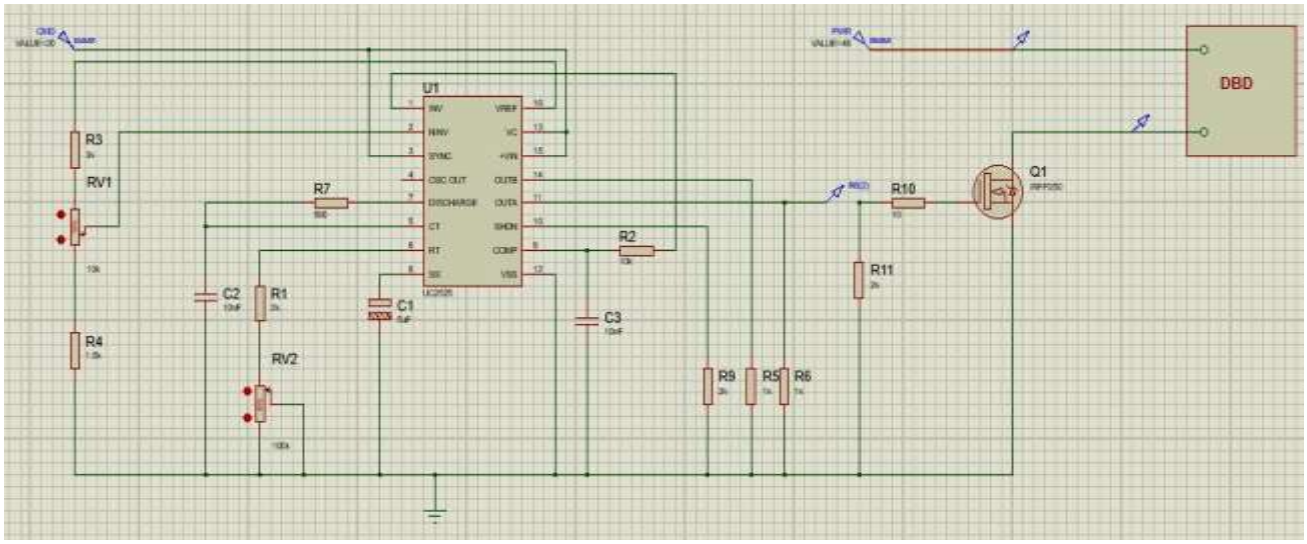

Figure 4.5. Complete diagram of the SG2525 circuit power supply, [74]

The results of the power supply simulation are presented in Figure 4.6. The voltage peaks are the result of the inductance of the primary winding.

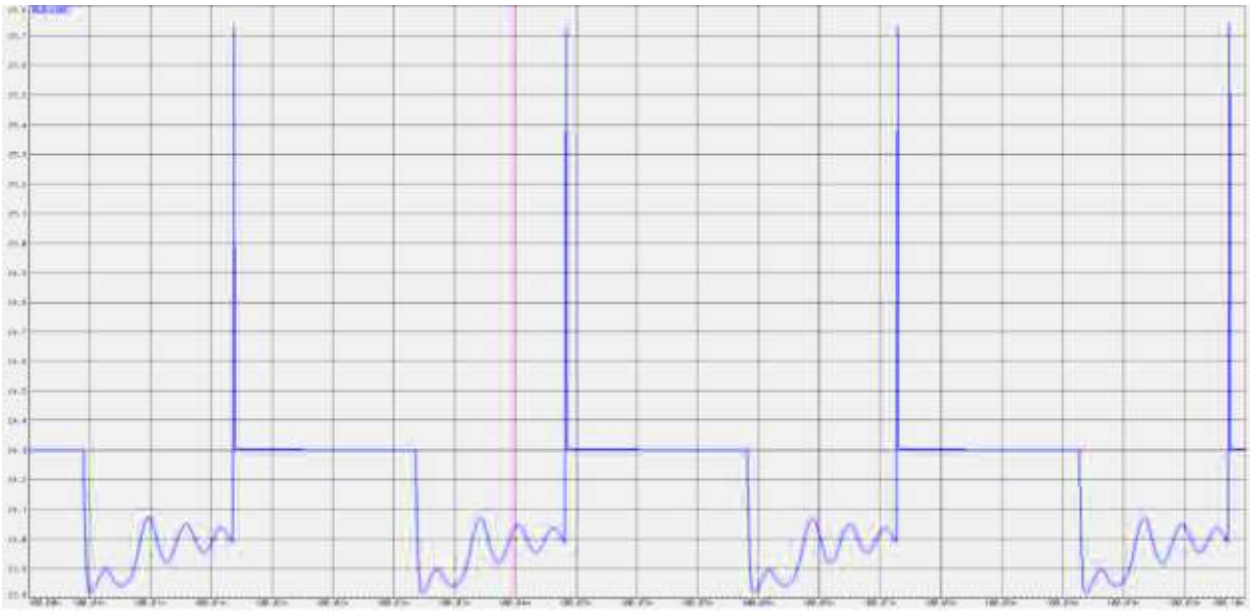

Figure 4.6. The result of simulating the power supply with the SG2525 circuit, [74]

The frequency range for this source is from 6kHz to 60 kHz, between the two outputs at pin 11 and pin 14. The two outputs oscillate alternately in push (totem) mode, driving the connected mosfet transistor in flyback configuration.

Because the integrated facilitates a PWM control pin-out, it can be exploited to allow automatic adjustment of the system output.

Pin 2 is the built-in internal error detection input, and normally the voltage at this non-reversing pin should not rise above the 5.1V value by default, because the inv # 1 pin is set to 5.1V by internal reference.

As long as pin 2 falls within the specified voltage limit, the PWM correction feature remains inactive, and yet when the voltage at pin 2 tends to rise above 5.1V, the output pulses are subsequently restricted, in trying to correct and balance the output voltage accordingly.

4.4. Types of DBD reactors used in the experimental part

Non-thermal plasma discharges are found in a number of interesting industrial applications in addition to ozone generation. Generation of strong infrared radiation in CO2 lasers and ultraviolet (UV) or ultraviolet vacuum (VUV) incineration in excimer lamps are examples of the latest developments in plasma.

Figure 4.7 below shows the DBD reactor topologies, of which 3 are planar and one is circular.

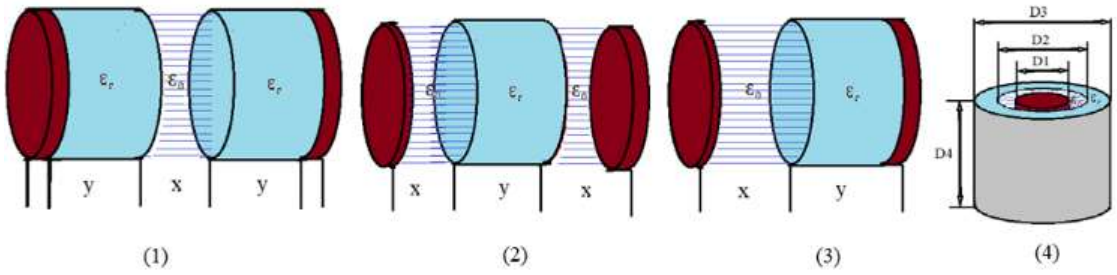

Figure 4.7. Typical dielectric barrier discharge electrode configurations

No blowing gas was used for these experiments, no special enclosure with any other gas, no ambient air was used (approximately 25 ° C).

Considering that the type of glass used is BBS for flat topology reactors and LBSCA for cylindrical topology, which have the value of relative permittivity.

Using these data, the calculations obtained will be presented below.

4.4.1. Dielectric reactor - air - dielectric considered as flat capacitor (Reactor 1)

For the topology shown in Figure 4.8, it is necessary to consider 3 equivalent capacitors calculated according to the dimensions of the respective glass insulating layer.

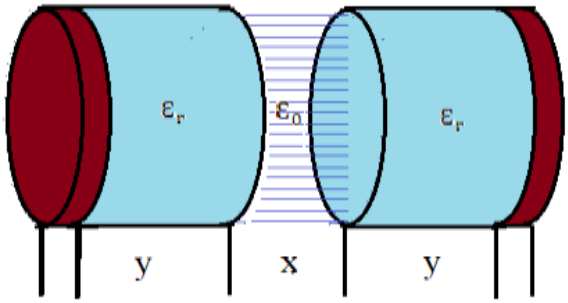

Figure 4.8. Equivalent scheme used in the calculation of equivalent capacity for DBD reactor dielectric - air - dielectric

The dimensions shown in Figure 4.8 are $y = 1.5\ mm$ și $x = 1\ mm$. For the calculation of the equivalent capacity, it is taken into account that there are 3 equivalent capacities grouped in series for each area delimited by the dielectric. Thus the equivalent capacity is:

$$C = \frac{C_1 C_2 C_3}{C_1 C_2 + C_2 C_3 + C_1 C_3} \tag{4.1}$$

Grounding electrode surface = 551.54 mm2, discharge space = 1 mm, upper dielectric thickness (glass) = 1.5 mm, lower dielectric thickness (glass) = 1.5 mm, high voltage electrode surface = 47.78 mm^2.

The result obtained for the static capacity of the dielectric reactor - air - dielectric is C = 1,947 pF.

4.4.2. Air reactor - dielectric - air considered as a flat capacitor (Reactor 2)

For the topology shown in Figure 4.9, it is necessary to consider 3 equivalent capacitors calculated according to the dimensions of the respective glass insulating layer. The dimensions are shown below.

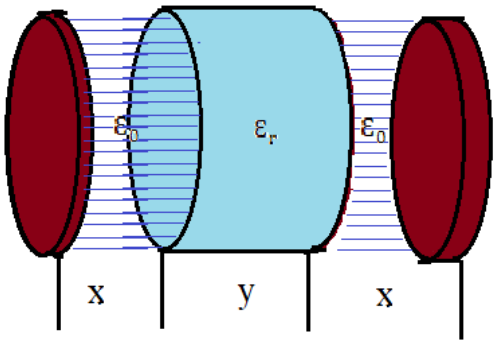

Figure 4.9. Equivalent reactor used in the calculation of equivalent capacity for DBD reactor air - dielectric - air,

The dimensions shown in Figure 4.9 are $y = 1.5\ mm$ și $x = 1\ mm$. For the calculation of the equivalent capacity, it is taken into account that there are 3 equivalent capacities for each area delimited by the dielectric. Thus the equivalent capacity is:

$$C = \frac{C_1 C_2 C_3}{C_1 C_2 + C_2 C_3 + C_1 C_3} \tag{4.2}$$

Grounding electrode surface = 551.54 mm2, discharge space = 1 mm, dielectric thickness = 1.5 mm, high voltage electrode surface = 47.78 mm^2.

The result obtained for the static capacity of the dielectric - air - dielectric reactor is C = 0.384 pF.

4.4.3. Air reactor - dielectric considered as flat capacitor (Reactor 3)

For equivalent calculation, the equivalent capacity with two flat capacitors connected in series must be taken into account. Depending on the permissiveness chosen, the calculations are presented below.

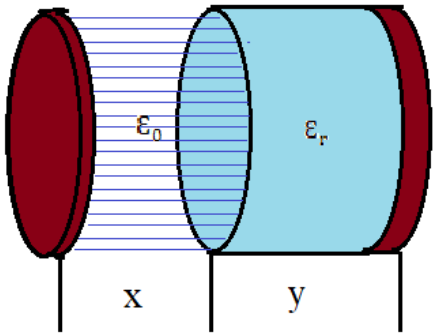

Figure 4.10. Equivalent scheme used in the calculation of the equivalent capacity for air-dielectric DBD reactor

The dimensions shown in Figure 4.10 are $y = 1.2\ mm$ și $x = 2.3\ mm$. For the calculation of the equivalent capacity, account shall be taken of the fact that there are two equivalent capacities for each dielectric bounded area. Thus the equivalent capacity is:

$$C = \frac{C_1 C_2}{C_1 + C_2} \tag{4.3}$$

Grounding electrode surface = 551.54 mm2, discharge space = 2 mm, dielectric thickness = 1.5 mm, high voltage electrode surface = 47.78 mm^2.

The result obtained for the static capacity of the dielectric - air - dielectric reactor is C = 0.19 pF.

4.4.4. Cylindrical reactor considered as cylindrical capacitor (Reactor 4)

The last reactor presented is the one in cylindrical configuration. The dimensions for this reactor are the inside diameter of the ground electrode = 7 mm, the outside diameter of the ground electrode = 9 mm, the discharge space (D2) = 1.5 mm, the thickness of the dielectric (D3) = 1.5 mm, the diameter of the HV electrode (D1) = 1.7 mm.

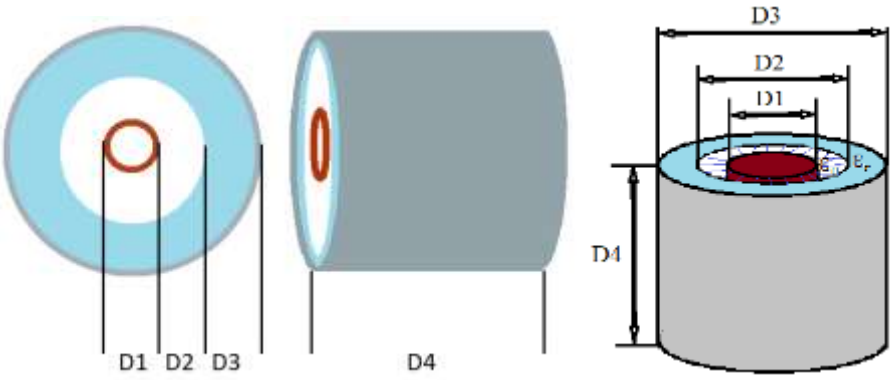

Figure 4.11. Representation of the experimental setup for the circular DBD reactor, [74]

The formula is used to calculate the cylinder capacity:

$$C = \frac{2\pi\varepsilon_0\varepsilon_r l}{ln\frac{R_e}{R_i}} \tag{4.4}$$

Where l - is the height of the cylinder, Re - is the outer diameter, Ri - is the inner diameter.

$$C_1 = \frac{2\pi\varepsilon_0 D_4}{ln\frac{D_2}{D_1}} \tag{4.5}$$

$$C_2 = \frac{2\pi\varepsilon_0\varepsilon_r D_4}{ln\frac{D_3}{D_2}} \tag{4.6}$$

Grounding electrode surface = 494.8 mm2, discharge space 1.7 mm, dielectric thickness (glass) = 1.5 mm, high voltage electrode surface = 350.35 mm^2.

The result obtained for the static capacity of the cylindrical reactor is C = 4.36 pF.

4.4.5. The experimental set of DBD reactors used

For experimental use, the configuration shown in the block diagram in Figure 4.12 was used. Here is how to connect the power supplies (with the power part and the control part respectively), the primary windings (which can be 10, 18 or 22) in series with a 4 Ω ceramic film power resistor and the connection of the probes to oscilloscope (probe that collects the voltage on the resistor to calculate the current on the primary / TESTEC HVP 40 probe with which the signal is collected from the reactor).

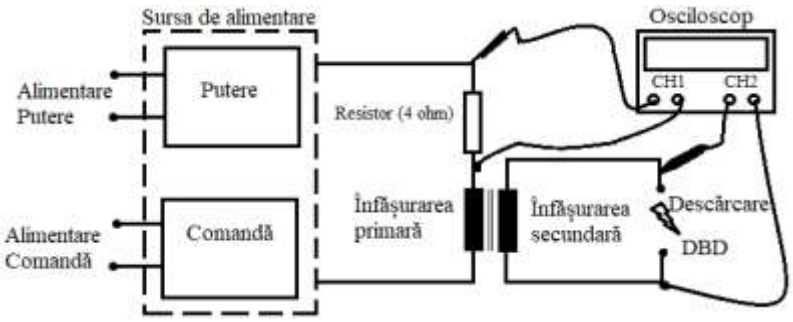

Figure 4.12. Block diagram of the experimental setup for connecting DBD reactors, [74]

With the help of these reactors, a series of experiments were performed with different parameters to determine the dynamic capacity and to highlight the contribution and efficiency of each source tested with these configurations.

CHAPTER 5. Experimental results on electrical parameters of discharges

The experiments performed with the two power supplies considered all 4 possible geometries of DBD type reactors. A transformer with 2500 windings for the secondary coil and 10, 18 and 22 windings for the primary one was used to produce the high voltage. To limit the current, the primary winding was connected in series with a 4 ohm power resistor. Data were collected using a 1000: 1 TT-HVP 40 offset high voltage probe from TESTEC.

DBD electric shocks, due to the multiple plasma channels and the fact that the discharge goes out quickly, require a high frequency for their maintenance. During the experimental part, the frequency had to be limited due to the saturation of the ferrite core and the limitations present in the MOSFET transistors used.

Since both power supplies operate at close frequencies and the same PWM modulation factor, the difference in amplitude is due to the difference between the half bridge topology and the flyback topology and the fact that each power supply operates at different power voltages for the power section.

At this stage the input parameters of the sources that were variable (adjusted) are:

-Control pulse frequency - by means of potentiometers connected to the inputs specific to the control integrated circuits, the frequencies used for the experimental base are 30 and 60 kHz respectively;

- Duty cycle - by means of potentiometers connected to the inputs specific to the control integrated circuits, which in this case are 20% and 50% respectively;

-The high voltage level applied to the DBD reactors by choosing a certain number of turns from the high voltage coil mayor. 10, 18 and 22 were used for this work, which allowed the modification of the transformation ratio and the obtaining of different voltage values in the secondary of the coil.

The adjustment of these input parameters was primarily aimed at obtaining an electric discharge as stable and homogeneous as possible on each of the reactor configurations used. At the same time, the aim was to reduce the demands on electronic components in switching during operation.

In addition to the parameters mentioned above, other equally important parameters, taken into account in the analysis presented, are the values of the dynamic capacity specific to the topology of the reactors.

In the literature this capacity has been measured experimentally using a capacitive divider connected to an oscilloscope. To determine these parameters in different cases Lissajous figures were used which provide a load type graph (Q) as a function of voltage (U). From these graphs the value of the capacity of the DBD reactor can be extracted.

In this paper we proceeded to another simplified approach for determining the capacity, we followed the variation of the frequency obtained after the download and we calculated the value of the dynamic capacity from the formula:

$$C=\frac{1}{4\pi^2 f^2 L} \qquad (5.1)$$

This calculation took into account the measured value of the coil secondary inductance of 65 uH, measured with PeakTech 2170 and also took into account the value of the relative permittivity of the glass used.

5.1. Experimental results obtained using the TL494 power supply

Taking into account the parameters considered for the experimental part of both sources, this subchapter will focus on the particularities of the source with TL494. The power supply parameters of the source are: 15V control supply voltage and 96V power supply voltage, both DC.

5.1.1. Electrical parameters measured for TL494 power supply

The parameters measured using the oscilloscope, namely the current on the primary of the transformer, respectively the output voltage depending on the reactor topology used, in the case of the primary with 10 windings are found in Tables 5.1 and 5.2 respectively.

Table 5.1. Primary current values in the case of the transformer with 10 primary windings

Parameters / Reactor	frequency 30 kHz		frequency 60 kHz	
	PWM 20%	PWM 50%	PWM 20%	PWM 50%
Reactor 1	9,64 [A]	8,43 [A]	6,75 [A]	6,71 [A]
Reactor 2	9,57 [A]	7,37 [A]	7,00 [A]	6,44 [A]
Reactor 3	9,74 [A]	8,14 [A]	6,71 [A]	6,69 [A]
Reactor 4	8,65 [A]	8,02 [A]	6,75 [A]	6,33 [A]

Table 5.1 shows that the highest values were obtained for reactors 1, 2 and 3 at the frequency of 30 kHz and a filling factor of 20% while the minimum values were obtained for all reactors at the frequency of 60 kHz using a filling factor of 50%. These values are due to the saturation of the ferrite core of the high voltage transformer, which reaches saturation due to the higher frequency at which these experiments were performed.

For the output voltage values (high voltage) the collected data are presented in Table 5.2. DBD discharges depend on the applied voltage and current limitation. Thus the values obtained are of the order of 4 kV for reactors 1,2 and 3 at a frequency of 30 kHz and a filling factor of 20% and up to 2 kV for all reactors at a frequency of 60 kHz and a filling factor of 50%, which is expected taking into account the power transfer.

Table 5.2. Output voltage values for transformer with 10 primary windings

Parameters / Reactor	frequency 30 kHz		frequency 60 kHz	
	PWM 20%	PWM 50%	PWM 20%	PWM 50%
Reactor 1	3647,60 [V]	3150,76 [V]	1792,99 [V]	1793,88 [V]
Reactor 2	3643,23 [V]	4318,64 [V]	2043,89 [V]	1880,89 [V]
Reactor 3	4884,39 [V]	4062,43 [V]	2357,49 [V]	2446,50 [V]
Reactor 4	4249,67 [V]	3086,45 [V]	1956,96 [V]	1845,16 [V]

From these values the energy transfer is observed, namely the current on the primary proportional to the voltage on the secondary. The values are proportional to the number of primary windings and implicitly to the transformation ratio.

Next, the case of the primary winding consisting of 18 turns was analyzed, the data collected being presented in Tables 5.3 and 5.4.

Taking into account the ratio of the windings and the value of the impedance, which in this case has increased, a decrease of the current per mayor is observed, and these values are presented in Table 5.3.

Table 5.3. Primary current values in the case of the transformer with 18 primary windings

Parameters / Reactor	frequency 30 kHz		frequency 60 kHz	
	PWM 20%	PWM 50%	PWM 20%	PWM 50%
Reactor 1	4,07 [A]	4,08 [A]	2,38 [A]	2,40 [A]
Reactor 2	4,24 [A]	4,17 [A]	7,00 [A]	7,00 [A]
Reactor 3	4,12 [A]	4,13 [A]	2,70 [A]	2,79 [A]
Reactor 4	3,81 [A]	3,84 [A]	2,44 [A]	2,42 [A]

The current values for this case are significantly lower than in the previous case (10 primary windings), and correspond to values of the output voltage close to reactors 1 and 3, where the maximum values at the frequency of 30 kHz and factor are obtained in this case as well. 20% filling.

For reactor 2, at the same parameters, the voltage value differs more than the previous case, which is due to the architecture of the reactor which has a thicker dielectric layer compared to other topologies. When using the 60 kHz frequency a similar decrease of values is observed only in this case the values are lower.

Table 5.4. Output voltage values for transformer with 18 primary windings

Parameters / Reactor	frequency 30 kHz		frequency 60 kHz	
	PWM 20%	PWM 50%	PWM 20%	PWM 50%
Reactor 1	2717,57 [V]	2727,58 [V]	1162,28 [V]	1159,38 [V]
Reactor 2	2960,31 [V]	3001,96 [V]	1424,68 [V]	1424,68 [V]
Reactor 3	3858,57 [V]	4062,65 [V]	2070,7 [V]	2073,49 [V]
Reactor 4	2712,47 [V]	2720,6 [V]	1255,39 [V]	1308,8 [V]

The third case analyzed is with the primary winding consisting of 22 turns. As can be seen from Tables 5.5 and 5.6, both the values of the output voltage and the value of the current measured in the primary decrease. Considering that the output consists practically of a voltage divider and that the reactance value changes depending on the inductance of the primary (default of the number of turns), the transformation ratio decreases, but also the voltage drop on the primary winding must be taken into account, which due to the value of the inductive reactance is higher.

The values of the current on the primary of the transformer are presented in table 5.5, where the effect of the increase of the inductive reactance on the primary is observed, namely the decrease of the current.

Table 5.5. Primary current values in the case of the transformer with 22 primary windings

Parameters / Reactor	frequency 30 kHz		frequency 60 kHz	
	PWM 20%	PWM 50%	PWM 20%	PWM 50%
Reactor 1	3,29 [A]	3,29 [A]	2,02 [A]	1,98 [A]
Reactor 2	3,43 [A]	3,39 [A]	2,02 [A]	2,01 [A]
Reactor 3	3,35 [A]	3,35 [A]	2,22 [A]	2,23 [A]
Reactor 4	3,21 [A]	3,19 [A]	2,14 [A]	2,33 [A]

For the values of the output voltage, in the case presented (22 primary windings) a decrease proportional to the increase in the number of turns is observed in table 5.6, due to the change of the transformation ratio.

Table 5.6. Output voltage values for transformer with 22 primary windings

Parameters / Reactor	frequency 30 kHz		frequency 60 kHz	
	PWM 20%	PWM 50%	PWM 20%	PWM 50%
Reactor 1	2717,56 [V]	2553,10 [V]	1252,26 [V]	1249,34 [V]
Reactor 2	2789,77 [V]	2681,95 [V]	1272,36 [V]	1263,25 [V]
Reactor 3	3619,06 [V]	3619,06 [V]	1859,67 [V]	1856,23 [V]
Reactor 4	2726,04 [V]	2795,67 [V]	1402,72 [V]	1672,35 [V]

The variations presented above in the other two cases (10 and 18 primary windings respectively) are proportional to those in this case, the only difference being the value which, although close, is smaller.

5.1.2. Dynamic capacity calculation for TL494 power supply

Most DBD discharges are symmetrical, and the voltage oscillates with the same frequency in both the positive and negative half-alternations. The frequency values were extracted from the experimental base with the help of which the dynamic capacity values were calculated.

The values obtained for the dynamic capacity obtained from the frequency measurement are presented centrally in Table 5.7.

Table 5.7. Dynamic capacity values for experiments performed with source TL494

Parameters / Reactor		frequency 30 kHz		frequency 60 kHz	
		PWM 20%	PWM 50%	PWM 20%	PWM 50%
Reactor 1	10 windings	0,67 pF	0,97 pF	0,43 pF	0,97 pF
	18 windings	1,32 pF	1,73 pF	0,97 pF	0,97 pF
	22 windings	0,43 pF	0,67 pF	0,67 pF	1,32 pF
Reactor 2	10 windings	0,97 pF	0,43 pF	0,67 pF	0,67 pF
	18 windings	0,97 pF	0,97 pF	1,32 pF	0,97 pF
	22 windings	0,97 pF	0,97 pF	0,97 pF	0,43 pF
Reactor 3	10 windings	0,43 pF	0,67 pF	0,24 pF	0,67 pF
	18 windings	1,32 pF	1,32 pF	0,97 pF	0,97 pF
	22 windings	0,97 pF	0,43 pF	0,97 pF	0,43 pF
Reactor 4	10 windings	0,43 pF	0,67 pF	0,24 pF	0,97 pF
	18 windings	1,32 pF	0,97 pF	0,97 pF	0,97 pF
	22 windings	0,67 pF	0,97 pF	0,97 pF	0,67 pF

The values of the download frequencies are between 20 and 30 MHz, which means that the dynamic capacity values are between 0.43 and 1,73 pF.

5.2. Experimental results obtained using SG2525 power supply

The electrical supply parameters of the source built with the SG2525 integrated circuit are: supply voltage for the control part 20V and supply voltage of the power circuit is 48V, both in d.c. At the same time it must be considered that in this case the fact that the voltage has only a positive polarity.

5.2.1. Electrical parameters measured for SG2525 power supply

Tables 5.8 and 5.9 show the parameters of primary current and output voltage in the case of the primary winding consisting of 10 turns.

The values of the currents shown in Table 5.8 vary between 0.8 and 6.64 A. The minimum current value was recorded for reactor 3 at 30 kHz and a fill factor of 20% and the maximum current was obtained for reactor 1 at frequency 30kHz and 50% fill factor.

Table 5.8. Primary current values in the case of the transformer with 10 primary windings

Parameters / Reactor	frequecy 30 kHz		frequecy 60 kHz	
	PWM 20%	PWM 50%	PWM 20%	PWM 50%
Reactor 1	3,12 [A]	6,64 [A]	4,42 [A]	3,41 [A]
Reactor 2	3,12 [A]	5,85 [A]	2,15 [A]	3,53 [A]
Reactor 3	0,79 [A]	5,57 [A]	2,70 [A]	5,21 [A]
Reactor 4	4,08 [A]	3,39 [A]	4,97 [A]	2,47 [A]

In this case, the maximum values of the voltage do not correspond to the maximum values of the currents, as in the case of the values extracted with the source built with the integrated circuit TL494. Thus for reactor 2 at a frequency of 30kHz and a filling factor of 20%, the current value is 3.12 A, this value corresponds to a voltage value of 9541.7 V. For the same reactor at the same frequency, but with a filling factor of 50 %, the values are 5.85A and the voltage is 4702.2V.

Table 5.9. Output voltage values for transformer with 10 primary windings

Parameters / Reactor	frequency 30 kHz		frequency 60 kHz	
	PWM 20%	PWM 50%	PWM 20%	PWM 50%
Reactor 1	5820,54 [V]	3838,12 [V]	1033,74 [V]	1962,04 [V]
Reactor 2	9541,74 [V]	4702,2 [V]	1899,44 [V]	1987,82 [V]
Reactor 3	4761,28 [V]	5120,26 [V]	1768,74 [V]	2461,24 [V]
Reactor 4	4761,28 [V]	4483,18 [V]	715,24 [V]	1524,65 [V]

Tables 5.10 and 5.11 show the primary current and the output voltage when using the SG2525 power supply in the case of the primary winding consisting of 18 turns.

Table 5.10. Primary current values in the case of the transformer with 18 primary windings

Parameters / Reactor	frequency 30 kHz		frequency 60 kHz	
	PWM 20%	PWM 50%	PWM 20%	PWM 50%
Reactor 1	2,91 [A]	4,46 [A]	3,78 [A]	4,20 [A]
Reactor 2	4,29 [A]	5,65 [A]	1,67 [A]	4,08 [A]
Reactor 3	4,04 [A]	5,07	2,38 [A]	4,70 [A]
Reactor 4	1,50 [A]	2,34 [A]	2,34 [A]	5,30 [A]

Table 5.11. Output voltage values for transformer with 18 primary windings

Parameters / Reactor	frequency 30 kHz		frequency 60 kHz	
	PWM 20%	PWM 50%	PWM 20%	PWM 50%
Reactor 1	4553,10 [V]	4489,28 [V]	3207,94 [V]	7536,67 [V]
Reactor 2	4416,59 [V]	3500,72 [V]	2074,97 [V]	6745,25 [V]
Reactor 3	4429,29 [V]	4178,01 [V]	3407 [V]	7511,22 [V]
Reactor 4	3489,60 [V]	4942,12 [V]	4942,12 [V]	5466,65 [V]

Tables 5.12 and 5.13 show the output parameters for the use of the SG2525 power supply in the case of the 22-turn primary winding.

Table 5.12. Primary current values in the case of the transformer with 22 primary windings

Parameters / Reactor	frequency 30 kHz		frequency 60 kHz	
	PWM 20%	PWM 50%	PWM 20%	PWM 50%
Reactor 1	9,81 [A]	2,01 [A]	3,35 [A]	3,79 [A]
Reactor 2	3,88 [A]	2,85 [A]	3,31 [A]	4,84 [A]
Reactor 3	2,95 [A]	2,27 [V]	2,17 [A]	4,22 [A]
Reactor 4	1,42 [A]	1,88 [V]	3,91 [A]	3,79 [A]

Table 5.13. Output voltage values for transformer with 22 primary windings

Parameters / Reactor	frequency 30 kHz		frequency 60 kHz	
	PWM 20%	PWM 50%	PWM 20%	PWM 50%
Reactor 1	5585,88 [V]	4481,68 [V]	5752,63 [V]	6765,54 [V]
Reactor 2	4855,16 [V]	4000,48 [V]	2113,89 [V]	4550,01 [V]
Reactor 3	4260,93 [V]	5089,36 [V]	2642,21 [V]	7955,38 [V]
Reactor 4	3764,24 [V]	4626,25 [V]	5091,55 [V]	981,35 [V]

5.2.2. Dynamic capacity calculation for SG2525 power supply

For the SG2525 source, the DBD discharges are asymmetric. The experimental basis, in this case, shows frequency values for some cases, in some cases no discharges occurred. The dynamic capacitance values were calculated using the download frequencies.

The values obtained for the dynamic capacity obtained from the frequency measurement are presented centrally in Table 5.14.

Tabelul 5.14. Valorile capacității dinamice pentru experimentele efectuate cu sursa SG2525

Parameters / Reactor		frequency 30 kHz		frequency 60 kHz	
		PWM 20%	PWM 50%	PWM 20%	PWM 50%
Reactor 1	10 windings	21,21 pF	-	-	0,43 pF
	18 windings	3,89 pF	-	-	0,24 pF
	22 windings	-	-	-	-
Reactor 2	10 windings	15,58 pF	15,58 pF	-	0,24 pF
	18 windings	15,58 pF	27,71 pF	-	0,67 pF
	22 windings	15,58 pF	21,21 pF	-	0,43 pF
Reactor 3	10 windings	15,58 pF	21,21 pF	-	0,43 pF
	18 windings	21,21 pF	15,58 pF	-	0,24 pF
	22 windings	6,92 pF	15,58 pF	0,43 pF	0,24 pF
Reactor 4	10 windings	21,21 pF	21,21 pF	-	-
	18 windings	27,71 pF	21,21 pF	0,43 pF	0,43 pF
	22 windings	15,58 pF	10,82 pF	0,67 pF	0,43 pF

The values of the download frequencies are between 5 and 30 MHz which means that the dynamic capacity values are between 0.43 and 21.21 pF.

Conclusions

This doctoral thesis concludes with the following findings:

- cold plasma, can be produced by different types of laboratory electrical discharges, such as GlidArc and dielectric barrier discharges (DBD).
- Limiting the current to values below 1A does not allow the evolution of the electric discharge towards the electric arc, which would mean a substantial increase in the temperature of the plasma particles.
- Direct, low, medium or high frequency or pulsed AC power supplies can be used to produce cold plasma.
- In addition to the construction of the reactor, power supplies also play a very important role in increasing the efficiency of cold plasma discharges.
- The use of these sources is especially useful for DBD-type discharges, which due to the multiple plasma channels and the fact that the discharge is quickly extinguished by the disappearance of the active species produced, requires a high frequency for their maintenance and implicitly discharges.
- Two power supplies have been designed to perform the experimental part, with the help of which DBD type electric discharges can be modeled.
- For the 4 DBD reactor topologies considered, the static capacity was calculated, which expresses the value depending on the distance between the electrodes and the dielectric used. It is a parameter that defines the DBD discharge and affects the electrical parameters of the discharge.
- An important issue with DBD discharges is the capacity that occurs in the reactor. Considering the 4 topologies presented in this paper, the data necessary for the calculation of the dynamic values of the capacity were extracted.
- The frequency for both power supplies is 30 and 60 kHz, the measured download frequency is between 15 MHz and 40 MHz for the TL494 power supply and between 5 MHz and 40 MHz for the SG2525 power supply. The determination of the dynamic capacity, in this study, is based on the measurement of the voltage of the discharge peak of its frequency and the knowledge of the value of the inductance of the secondary winding.
- The best discharge of DBD, in terms of the conditions of occurrence and the parameters necessary for priming and maintenance, took place in the tubular reactor, mainly due to the use of the internal copper electrode and the external aluminum electrode which ensured a good emissivity of ELECTRON.

References

[1] S. D. Anghel, *Fizica plasmei și aplicații*. Cluj-Napoca: Universitatea „Babeș-Bolyai” Cluj-Napoca.

[2] I. I. Popescu, I. Iova, and E. Toader, *Fizica plasmei și aplicații*. București: Editura Stiintifica si Enciclopedica, 1981.

[3] G. POPA and L. SIRGHI, *Bazele Fizicii Plasmei*. Iași: Facultatea de Fizica,Universitatea “Al. I. Cuza,” 2000.

[4] I. I. Popescu and D. St. Ciobotaru, *Bazele fizicii plasmei*. Editura Tehnică, 1987.

[5] S. Dan ANGHEL SIMON Alpár, “PLASMA DE ÎNALTÃ FRECVENÞÃ,” 2002.

[6] R. Fitzpatrick, “Introduction to Plasma Physics: A graduate level course,” *Univ. Texas Austin, Austin, TX*, p. 242, 2006.

[7] Hnatiuc Eugen, *PROCEDES ELECTRIQUES DE MESURE ET DE TRAITEMENT DES POLLUANTS*. Franța: Tec & Doc Lavoisier, 2002.

[8] B. Hnatiuc, E. Hnatiuc, S. Pellerin, and J. Chapelle, “Experimental analysis of a double-spark ignition system,” *Czechoslov. J. Phys*, vol. 56, no. 8, pp. 851–867, 2006, doi: 10.1007/s10582-006-0135-1.

[9] U. Kogelschatz, “Fundamentals and applications of dielectric-barrier discharges FUNDAMENTALS AND APPLICATIONS OF DIELECTRIC-BARRIER DISCHARGES,” no. May, 2000.

[10] E. Hnatiuc and B. Hnatiuc, *Aparate electrice*. Constanța: Editura Tehnopress, 2011.

[11] G. Hortopan, G. Cosmin, and V. Panaite, *Aparate electrice de joasă tensiune*. București: Editura Tehnică, 1969.

[12] Hnatiuc Bogdan, *APARATE ELECTRICE. Îndrumar de aplicații*. Constanța: Nautica, 2016.

[13] B. HNATIUC, A. SABĂU, S. GHIȚĂ, M. HNATIUC, C. L. DUMITRACHE, S. ZĂGAN, “TRATAMENTE CU PLASMĂ NON-TERMICĂ PENTRU APLICAȚII DIN DOMENIUL NAVAL,” no. 4, 2014.

[14] A. Sabău, B. Hnatiuc, S. GHIȚĂ, and M. HNATIUC, “MĂSURAREA PUTERII UTILE LA TRATAMENTELE CU PLASMĂ NON-TERMICĂ,” *Bul. AGIR, Supl. 3/2016*, vol. 2, pp. 108–112, 2016.

[15] I. C. Felea, *STUDIUL POSIBILITĂȚILOR DE UTILIZARE A REACTORULUI DE TIP GLIDARC PENTRU BIODECONTAMINARE ÎN INSTALAȚII DE CONDIȚIONARE A AERULUI*. Iași: UNIVERSITATEA TEHNICĂ „GHEORGHE ASACHI” DIN IAȘI FACULTATEA DE INGINERIE ELECTRICĂ, ENERGETICĂ ȘI INFORMATICĂ APLICATĂ, 2019.

[16] Y. P. Raizer, *Gas discharge Physics*. Moscova, 1991.

[17] C.-V. LUNGU and Bogdan HNATIUC, “STUDIUL COMPARATIV AL UNOR SURSE DE ALIMENTARE FOLOSITE PENTRU PRODUCEREA DESCĂRCĂRILOR ELECTRICE DE TIP PLASMĂ RECE,” *Bul. AGIR nr. 4/2017 octombrie-decembrie*, vol. 4, 2017.

[18] Dragos-george Astanei and Hnatiuc Bogdan, “Surse de alimentare in impulsuri folosite pentru descarcari electrice de tip plasma rece,” 2000.

[19] E. Hnatiuc, J. Brisset, B. Hnatiuc, R. Burlica, and C. Roman, “About electrochemical reactors with cold plasma discharges engineering,” in *European Research in Cold Plasma Applications Conference, Iasi*, 2007, pp. 99–126.

[20] J. L. Brisset *et al*, “Chemical Reactivity of Discharges and Temporal Post-Discharges in Plasma Treatment of Aqueous Media: Examples of Gliding Discharge Treated

Solutions," *Ind. Eng. Chem. Res*, vol. 47, no. 16, pp. 5761–5781, 2008, doi: 10.1021/ie701759y.
[21] F. Peeters and T. Butterworth, "Electrical Diagnostics of Dielectric Barrier Discharges," in *Atmospheric Pressure Plasma - from Diagnostics to Applications*, no. tourism, IntechOpen, 2019, p. 13.
[22] C. dr ing Bogdan HNATIUC, Șl dr ing Adrian SABĂU, L. dr Simona GHIȚĂ, C. dr ing Mihaela HNATIUC, D. ing Remus ZĂGAN, and C. dr Eugen DUMITRU, "PRODUCEREA APEI ACTIVATE CU PLASMĂ PENTRU APLICAȚII DE DECONTAMINARE," *Bul. AGIR nr. 4/2015 ● octombrie-decembrie*.
[23] D. G Astanei and B. Hnatiuc, "Surse de alimentare in impulsuri folosite pentru descarcari electrice de tip plasma rece," 2000.
[24] "Descărcare barieră dielectrică (DBD) | Institutul de Inginerie a Proceselor Interfaciale și Tehnologia Plasmei Universitatea din Stuttgart." https://www.igvp.uni-stuttgart.de/en/research/plasma-technology/sources/barrier/ (accessed Aug. 31, 2021).
[25] M. Cojan, A. Simion, and L. M. Livadaru, "PROCEDEU DE OBȚINERE A PLASMEI RECI, TIP ARC GLISANT," 95-01767A, 1997.
[26] B. Hnatiuc, A. Sabau, C. Petrescu, and M. Wartel, "Characterization of different types of gliding discharges: Electrical parameters and breakdown simulation," *Proc. 2016 Int. Conf. Expo. Electr. Power Eng. EPE 2016*, pp. 102–105, 2016, doi: 10.1109/ICEPE.2016.7781312.
[27] C. Ferrand, *Caractérisation de sources plasmas dédiées à la simulation de rentrées atmosphériques et au traitement de polluants : arc soufflé basse pression et décharge glissante atmosphérique*. 2004.
[28] J. L. Brisset and E. Hnatiuc, "Peroxynitrite: A re-examination of the chemical properties of non-thermal discharges burning in air over aqueous solutions," *Plasma Chem. Plasma Process*, vol. 32, no. 4, pp. 655–674, Aug. 2012, doi: 10.1007/s11090-012-9384-x.
[29] S. P. S. Ghiță, J.-M. Herryb, B. Hnatiuca, M. Guilbaudb, M. Hnatiuca, A. Sabăua, F. Faubertc, M. Wartelc, "Influence of the Non-Thermal Plasma Treatment Concerning the Growth of Microorganisms on a Naval Steel Surface," *Biofouling*, pp. 1–17, 2006.
[30] H. D. Stryczewska, "Supply systems of non-thermal plasma reactors. Construction review with examples of applications," *Applied Sciences (Switzerland)*, vol. 10, no. 9. Multidisciplinary Digital Publishing Institute, p. 3242, May 07, 2020, doi: 10.3390/app10093242.
[31] R. Burlica, B. Hnatiuc, E. Hnatiuc, and M. Ursachi, "Effect of electrical current on H2/ H2O2 generation in non-thermal plasma gliding arc reactors," *Environ. Eng. Manag. J*, vol. 10, no. 4, pp. 579–585, 2011, doi: 10.30638/eemj.2011.080.
[32] M. Moreau *et al*, "Gliding Arc Discharge in the Potato Pathogen Erwinia carotovora subsp. atroseptica : Mechanism of Lethal Action and Effect on Membrane-Associated Molecules," *Appl. Environ. Microbiol*, vol. 73, no. 18, pp. 5904–5910, Sep. 2007, doi: 10.1128/AEM.00662-07.
[33] E. Hnatiuc and B. Hnatiuc, "Sistem multielectrod pentru realizarea reactoarelor electrochimice cu plasmă rece și circuit pentru comanda și reglarea funcționării acestuia," 112225B, 1996.
[34] A. Czernichowski, B. Hnatiuc, P. Pastva, and A. Ranaivosoloarimanana, "Générateurs et circuits électriques pour alimenter des décharges instables de haute tension," FR2817444A1 în Franța, US2002093294 în S.U.A, 2000.
[35] R. Burlica, E. Hnatiuc, B. Hnatiuc, and M. I. URSACHE, "DISPOZITIV CU PLASMĂ RECE ȘI ELECTROZI NESIMETRICI DESTINAT REFORMĂRII COMPUȘILOR ORGANICI ÎN VEDEREA OBȚINERII HIDROGENULUI," RO

128078 B1, 2017.
[36] E. Hnatiuc, J. L. Brisset, and B. Hnatiuc, “The ignition and control condition for the useful discharge in a glidarc reactor with plane geometry and auxiliary electrodes,” *Proc. Int. Conf. Optim. Electr. Electron. Equipment, OPTIM*, pp. 1349–1354, 2010, doi: 10.1109/OPTIM.2010.5510550.
[37] A. Czernichowski, “Plasmas pour la destruction de l’H2S et des mercaptans,” *Oil Gas Sci. Technol*, vol. 54, no. 3, pp. 337–355, May 1999, doi: 10.2516/OGST:1999031.
[38] L. Jaroszyński, “Computer simulation of the supply systems of the gliding arc plasma reactors,” *4 th Int. Conf. ELMECO*, no. September 2003, pp. 109–114, 2003.
[39] L. Jaroszyński and H. D. Stryczewska, “Numerical Analysis of the Integrated Supply System of Glidarc Plasma Reactor,” no. June, 1990, doi: 10.13140/2.1.1794.9124.
[40] R. Burlica and B. R. Locke, “Pulsed plasma gliding-arc discharges with water spray,” *IEEE Trans. Ind. Appl*, vol. 44, no. 2, pp. 482–489, 2008, doi: 10.1109/TIA.2008.916603.
[41] I. D. Dirlau, R. Burlica, and D. Ș. Astanei, “EFFECT OF NON-THERMAL PLASMA ON MOLECULAR SPECIES FORMED IN WATER BASED SOLUTION,” *Bul. INSTITUTULUI Politeh. DIN IAȘI*, vol. 63, no. 67, pp. 10–20, 2017.
[42] B. Hnatiuc, M. Hnatiuc, C. Petrescu, and D. Astanei, “Ignition modelling of a double sparking plug for internal combustion engines,” *EPE 2014 - Proc. 2014 Int. Conf. Expo. Electr. Power Eng*, pp. 226–230, 2014, doi: 10.1109/ICEPE.2014.6969902.
[43] “Cum se fabrica bujiile cu scânteie? - Denso.” https://www.denso.ro/noutăți/știri-corporate/2016/cum-se-fabrica-bujiile-cu-scanteie/ (accessed Aug. 31, 2021).
[44] B. Hnatiuc, A. Sabau, and D. Astanei, “Classic spark simulation using COMSOL software,” *IOP Conf. Ser. Mater. Sci. Eng*, vol. 591, no. 1, Aug. 2019, doi: 10.1088/1757-899X/591/1/012050.
[45] S. K. Sharma and A. Shyam, “Design and testing of 45 kV, 50 kHz pulse power supply for dielectric barrier discharges,” *Rev. Sci. Instrum*, vol. 87, no. 10, 2016, doi: 10.1063/1.4964507.
[46] “MOSFET 48N50 .” https://www.digchip.com/datasheets/parts/datasheet/244/48N50-pdf.php (accessed Sep. 01, 2021).
[47] H. T. Truong, M. Hayashi, Y. Uesugi, Y. Tanaka, and T. Ishijima, “Novel design of high voltage pulse source for efficient dielectric barrier discharge generation by using silicon diodes for alternating current,” *Rev. Sci. Instrum*, vol. 88, no. 6, 2017, doi: 10.1063/1.4984947.
[48] “Agilent Technologies InfiniiVision 6000L Series Low-Profile Oscilloscopes The most space efficient , and affordable LXI C compliant oscilloscopes Four channels in only 1U space.” http://www.distek.ro/en/Product/Agilent-DSO6054L-Modular-Oscilloscope-4-x-500-MHz-380.
[49] S. Kalisiak, T. Jakubowski, and M. Balcerak, “Power Electronic Supply Systems For Non-Thermal Plasma Sources Outline :,” pp. 6–10, 2010.
[50] “Modul în care circuitul de conversie a convertorului pfc îmbunătățește calitatea alimentării - Știri 2021.” https://ro.answersexpress.com/how-boost-pfc-converter-circuit-improves-power-quality-55256 (accessed Aug. 31, 2021).
[51] D. STAICU, *SISTEME CRISTALE LICHIDE-POLIMERI. METODE FIZICE DE ANALIZĂ - Teză de doctorat*. București: UNIVERSITATEA DIN BUCUREȘTI Facultatea de Fizică Școala Doctorală de Fizică, 2018.
[52] S. Gaur, G. Vergason, V. Technology, and V. Etten, “Plasma Polymerization: Theory and Practice,” *Soc. Vac. Coaters 43rd Annu. Tech. Conf. Proc*, pp. 267–271, 2000.
[53] S. D. ANGHEL and S. Alpár, *PLASMA DE ÎNALTĂ FRECVENȚĂ*. Cluj-Napoca: NapocaStar, 2002.

[54] M. Asandulesa, I. Topala, V. Pohoata, and N. Dumitrascu, “Influence of operational parameters on plasma polymerization process at atmospheric pressure,” *J. Appl. Phys*, vol. 108, no. 9, Nov. 2010, doi: 10.1063/1.3506528.
[55] “Tabor Electronics WW5064 .” https://www.taborelec.com/ww5064 (accessed Aug. 31, 2021).
[56] “Trek PD07016 | Amplificatoare de înaltă tensiune | Energie avansată.” https://www.advancedenergy.com/products/high-voltage-products/high-voltage-amplifiers/standard-high-speed-amplifiers/trek-PD07016/ (accessed Sep. 01, 2021).
[57] O. Levasseur *et al*, “Deposition of Hydrophobic Functional Groups on Wood Surfaces Using Atmospheric-Pressure Dielectric Barrier Discharge in Helium-Hexamethyldisiloxane Gas Mixtures,” *Plasma Process. Polym*, vol. 9, no. 11–12, pp. 1168–1175, Dec. 2012, doi: 10.1002/PPAP.201100222.
[58] D. Merche, N. Vandencasteele, and F. Reniers, “Atmospheric plasmas for thin film deposition: A critical review,” *Thin Solid Films*, vol. 520, no. 13. pp. 4219–4236, Apr. 30, 2012, doi: 10.1016/j.tsf.2012.01.026.
[59] O. Levasseur *et al*, “Deposition of hydrophobic functional groups on wood surfaces using atmospheric-pressure dielectric barrier discharge in helium-hexamethyldisiloxane gas mixtures,” *Plasma Process. Polym*, vol. 9, no. 11–12, pp. 1168–1175, 2012, doi: 10.1002/ppap.201100222.
[60] T. Kelley, “Agilent 33120A Signal Generator UTA Quick Guide.” https://cdn.web.uta.edu/-/media/project/website/engineering/electrical-department/_documents/agilent_33120a_signal_generator_guide_ver_1_00.ashx?revision=4d711a43-d110-4fd3-abdf-ea7f1ba087cd (accessed Aug. 31, 2021).
[61] N. Naudé, J.-P. Cambronne, N. Gherardi, and F. Massines, “Electrical model and analysis of the transition from an atmospheric pressure Townsend discharge to a filamentary discharge,” *J. Phys. D. Appl. Phys*, vol. 38, no. 4, p. 530, Feb. 2005, doi: 10.1088/0022-3727/38/4/004.
[62] M.-V. Teodorescu, *Surse de plasmă de radiofrecvenă cu barieră de dielectric - REZUMAT TEZĂ DE DOCTORAT*. UNIVERSITATEA DIN BUCUREȘTI Școala Doctorală de Fizică, 2012.
[63] D. C. TUDORAN, M. C. TUDORAN, and V. SURDUCAN, “REACTOR CU PLASMĂ RECE PENTRU OBȚINEREA COMBUSTIBILULUI BIODIESEL,” RO 131043 B1, 2021.
[64] G. Anastopoulos, Y. Zannikou, S. Stournas, and S. Kalligeros, “Transesterification of Vegetable Oils with Ethanol and Characterization of the Key Fuel Properties of Ethyl Esters,” vol. 2, pp. 362–376, 2009, doi: 10.3390/en20200362.
[65] “AT89S52 .” https://pdf1.alldatasheet.com/datasheet-pdf/view/82390/ATMEL/AT89S52.html (accessed Sep. 02, 2021).
[66] “βAA145 – Circuit de comanda in faza – Tehnium.org.” http://www.tehnium.org/2020/06/14/βaa145-circuit-de-comanda-in-faza/ (accessed Sep. 02, 2021).
[67] C. V Lungu and B. Hnatiuc, “Influence of the electric discharge and the power supply on the aqueous solution interface parameters,” in *IOP Conference Series: Materials Science and Engineering*, 2019, vol. 591, no. 1, doi: 10.1088/1757-899X/591/1/012054.
[68] “Bobina inductie pentru oltcit.” https://www.autopieseonline24.ro/citroen/oltcit/8295/10250/bobina_inductie (accessed Sep. 02, 2021).
[69] “Schema internă a transformatorului utilizat împreună cu sursa construită pe baza microcontroller-ului AT89S52.”

https://www.hrdiemen.com/reparation/flyback/scheme/7255 (accessed Sep. 02, 2021).
[70] L. C. Victor and H. Bogdan, “Cold Plasma Treatment Influence on Aqueous Solution Related to the Electrical Parameters of the Power Supply,” in *2019 International Conference on Electromechanical and Energy Systems, SIELMEN 2019 - Proceedings*, Oct. 2019, pp. 1–6, doi: 10.1109/SIELMEN.2019.8905791.
[71] M. J. Pavlovich *et al*, “Air spark-like plasma source for antimicrobial NOx generation,” *J. Phys. D. Appl. Phys*, vol. 47, no. 50, 2014, doi: 10.1088/0022-3727/47/50/505202.
[72] C. V. Lungu and B. Hnatiuc, “Simulation of power supplies used for nonlinear electrical discharges,” *Technium: Romanian Journal of Applied Sciences and Technology*, vol. 2, no. 1. pp. 79–84, 2020, doi: 10.47577/technium.v2i1.45.
[73] C. Victor and B. Hnatiuc, “Electrical simulation of discharges producing non-thermal plasma,” *Sci. Conf. Dr. Sch. SCDS-UDJG*, no. June, p. 2019, 2019.
[74] C. V Lungu and B. Hnatiuc, “DIELECTRIC BARRIER DISCHARGE ANALYSIS FROM THE POINT OF VIEW OF SUPPLY VOLTAGE AND REACTOR TOPOLOGY,” *Mod. Technol. Ind. Eng.*
[75] B. R. Priya Rani and M. T. Sebastian, “The effect of glass addition on the dielectric properties of barium strontium titanate,” *J. Mater. Sci. Mater. Electron*, vol. 19, no. 1, pp. 39–44, Jan. 2008, doi: 10.1007/S10854-007-9224-6.
[76] L. C. Victor, “Experimental determination of Dielectric Barier Discharge (DBD) type reactors capacity,” pp. 0–3.